Pilotins are mobile T3SS components involved in assembly and substrate specificity of the bacterial type III secretion system

Stephan Wimmi, Moritz Fleck*, Carlos Helbig, Corentin Brianceau, Katja Langenfeld, Witold G. Szymanski, Georgia Angelidou, Timo Glatter, Andreas Diepold*

Max Planck Institute for Terrestrial Microbiology, Department of Ecophysiology,

Karl-von-Frisch-Str. 10, 35043 Marburg, Germany

Corresponding author: Andreas Diepold, andreas.diepold@mpi-marburg.mpg.de,

+49-6421-178302

*: These authors contributed equally to this work

Short title: Pilotins contribute to T3SS assembly and substrate specificity

18

19 ## Abstract

20 In animal pathogens, assembly of the type III secretion system injectisome requires the presence of
21 so-called pilotins, small lipoproteins that assist the formation of the secretin ring in the outer
22 membrane. Using a combination of functional assays, interaction studies, proteomics and live-cell
23 microscopy, we determined the contribution of the pilotin to assembly, function and substrate
24 selectivity of the T3SS and identified potential new downstream roles of pilotin proteins. In the
25 absence of its pilotin SctG, *Yersinia enterocolitica* forms few, largely polar injectisome sorting
26 platforms and needles. In line, the majority of export apparatus subcomplexes is mobile in these
27 strains, suggesting the absence of fully assembled injectisomes. Remarkably, the export of late T3SS
28 substrates including the virulence effectors is hardly affected in these bacteria, whereas early T3SS
29 substrates, such as the needle subunits, are only exported to a very low degree. We found that
30 pilotins transiently interact with the secretin and the large export apparatus component SctV, but
31 mostly localize throughout the bacterial membrane, where they form transient mobile clusters,
32 which do not colocalize with assembled injectisomes. In addition, pilotins interact with non-T3SS
33 components, including sugar transporters. Pilotins therefore have additional functions downstream
34 injectisome assembly, which include the regulation of type III secretion and a potential new link to
35 the cellular energy metabolism.

36

37 # Introduction

38 Bacteria that live in contact to eukaryotic cells greatly benefit from being able to manipulate those
39 cells. The bacterial type III secretion system (T3SS) allows such manipulation by injecting effector
40 proteins directly from the bacterial cytosol into the host cell cytoplasm [1–5]. Although the T3SS is
41 also used by symbionts and commensals, it is best known for its essential role in infections of
42 important human pathogens such as *Salmonella*, *Shigella* and *Yersinia*. In these pathogens, the T3SS
43 machinery, also called injectisome[1], is often assembled upon entry into the host organism. Once the
44 basal body (membrane rings and export apparatus, Fig. 1a) and the cytosolic components are
45 assembled (reviewed in Diepold and Wagner, 2014), the T3SS starts to secrete its own distal
46 components. Amongst those so-called early secretion substrates are the subunits of the needle and
47 proteins required for its correct assembly, as well as early regulatory proteins. When the required
48 needle length is reached [7,8], middle secretion substrates – the translocon proteins forming the
49 needle tip and two hydrophobic interactors that build a pore in the host membrane – are secreted.
50 At this point, the injectisome is ready for secretion of the late secretion substrates, the virulence
51 effectors, which is initiated by host cell contact.

52 Injectisomes are assembled at the bacterial surface according to the needs of the bacteria in a given
53 situation. While in some cases, one to few injectisomes are sufficient (such as for the intracellular
54 *Salmonella* SPI-2 T3SS [9]), bacteria that need to actively make contact with the host cells usually
55 build more injectisomes [10,11]. The distribution of injectisomes across the bacterial surface is non-
56 random [12–14], but it is currently unclear what determines where new injectisomes are built.

57 A prime candidate to establish the site of assembly for new injectisomes is the pilotin, a lipoprotein
58 anchored in the inner leaflet of the outer membrane (OM). Pilotins are required for the proper
59 integration and oligomerization of the secretin protein, which forms a large channel in the OM in
60 the T3SS of animal pathogens, but also type II secretion systems (T2SS) and type IV pili (T4P) [15–
61 27]. Since the secretin ring is one of the nucleation structures of the injectisome [6,28] and anchors
62 the T3SS at its final position in the peptidoglycan mesh [29] (Fig. 1a), the localization of the pilotin
63 may determine the place of secretin ring formation and in consequence the distribution of
64 injectisomes.

[1] The T3SS is at the core of both injectisomes and bacterial flagella [11,96]. In this manuscript, "T3SS" refers to the injectisome-type, virulence-associated system.

65 Pilotins and their cognate secretin proteins in the T2SS and T3SS have been purified and structurally
66 analyzed in 1:1 complexes [23,30,31]. As a lipoprotein, the pilotin also interacts with the localization
67 of lipoproteins (Lol) protein export machinery [31,32]. Based on these properties, different models
68 for the export of the pilotin itself and its role in secretin ring assembly have been proposed [30,31].
69 Whether the pilotin stays attached to the secretin after secretin ring formation in the OM and the
70 subsequent assembly of the injectisome is debated and might differ between organisms. For T2SS
71 secretins, such attachment was initially proposed, but later rejected [23,33]; recent analyses of
72 purified secretin rings found pilotins attached stoichiometrically outside the main ring [34,35]. *In*
73 *situ* structures of the T3SS showed electron densities around the secretin, possibly corresponding
74 to pilotin proteins, in *Shigella flexneri* [36], but not in *Salmonella enterica* [37]. In spite of the
75 importance of pilotins for the localization of the central secretin ring structure, protein secretion by
76 the T3SS was found to be strongly impaired, but not completely prevented in absence of the pilotin
77 in some organisms [15,19,25] – the structural and mechanistic basis for this phenotype is currently
78 unclear.

79 Despite their central role, many key characteristics of pilotins are poorly understood or debated:
80 Why are pilotins usually not encoded with all other structural components of the T3SS, but upstream
81 the main transcription factor of the system? What determines their localization (and eventually that
82 of the injectisome)? Do pilotins remain part of the injectisome after the assembly and do they adapt
83 a functional role in type III secretion at this point?

84 To shed light on these questions and the role of pilotins in assembly and function of the T3SS, we
85 studied the role of the *Yersinia enterocolitica* pilotin SctG[2] with functional assays, fluorescence
86 microscopy, proteomics, as well as protein interaction and dynamics studies. We found that,
87 unexpectedly, SctG interacts with the secretin SctC only temporarily, and mostly localizes in dynamic
88 patches that are dispersed throughout the bacterial membrane. In absence of the pilotin, only a
89 small subset of bacteria assemble single, mostly polar needles which are not stably attached to fully
90 assembled injectisomes, as indicated by the lack of colocalization with the cytosolic sorting platform
91 component SctL. To our surprise, presence of the pilotin not only influenced injectisome assembly
92 and overall secretion levels, but specifically altered the secretion pattern of the T3SS. While effector
93 proteins and other late substrates were efficiently secreted in the absence of the pilotin, the export
94 of early substrates, such as the needle components, was greatly impaired. Based on specific

[2] This manuscript uses the common nomenclature for T3SS components [97,98]; the species-specific nomenclature of the *Yersinia* pilotin is YscW; other names can be found in Table S1.

95 interaction studies, we provide possible explanations for this unique phenotype and an extended
96 model for the function of the pilotin.

97

98 # Results

99 ## Deletion of the pilotin specifically reduces secretion of early export substrates

100 To define the overall role of the pilotin SctG in type III secretion, we tested the effects of a complete
101 *sctG* deletion on the virulence plasmid in *Y. enterocolitica* in a secretion assay. Absence of SctG
102 distinctly altered the secretion pattern. While secretion of effector proteins was partially reduced,
103 but still clearly present, early secretion substrates such as the needle subunit SctF, the ruler protein
104 SctP and translocators SctA, B, E were much more severely affected in secretion or not secreted at
105 all. *In trans* expression of SctG complemented the deletion (Fig. 1b, Fig. S1a).

106 In order to determine the role of SctG in secretion more precisely, we analyzed the secretome of
107 the wild-type and *ΔsctG* strains in minimal medium by label-free quantitative mass spectrometry.
108 The results show that T3SS substrates cluster according to their nature, rather than their overall
109 secretion level (Fig. 1c, Table 1, Fig. S1a): The late substrates, effector proteins YopH, O, P, E, M, T
110 as well as the gatekeeper SctW (YopN) and the negative regulators YscM1/2 (marked green in Fig.
111 1bc), were exported efficiently in absence of SctG. In clear contrast, export of all early and middle
112 substrates of the T3SS (marked magenta in Fig. 1bc) was strongly reduced in *ΔsctG*. These T3SS
113 substrates build up the needle (SctF) and the inner rod (SctI) connecting it to the export apparatus,
114 control needle length (SctP) and form its tip structure (SctA) as well as a pore in the host membrane
115 (SctB, E). YscX is an early T3SS substrate specific to the Ysc subgroup of T3SS [38,39], which is
116 required for the export of any other protein by the T3SS of the Ysc subgroup [40,41].

117 Since most pilotins, including SctG, are expressed in an operon with the main transcription factor of
118 the T3SS, VirF [42], we tested if the observed phenotype is caused by impaired VirF expression in
119 the absence of *sctG*. Expression of VirF from plasmid in a *ΔsctG* strain indeed slightly increased the
120 secretion of effectors, but not of early substrates (Fig. S1b), indicating that the specific loss of
121 secretion of these early substrates is not caused by an influence on VirF expression.

122

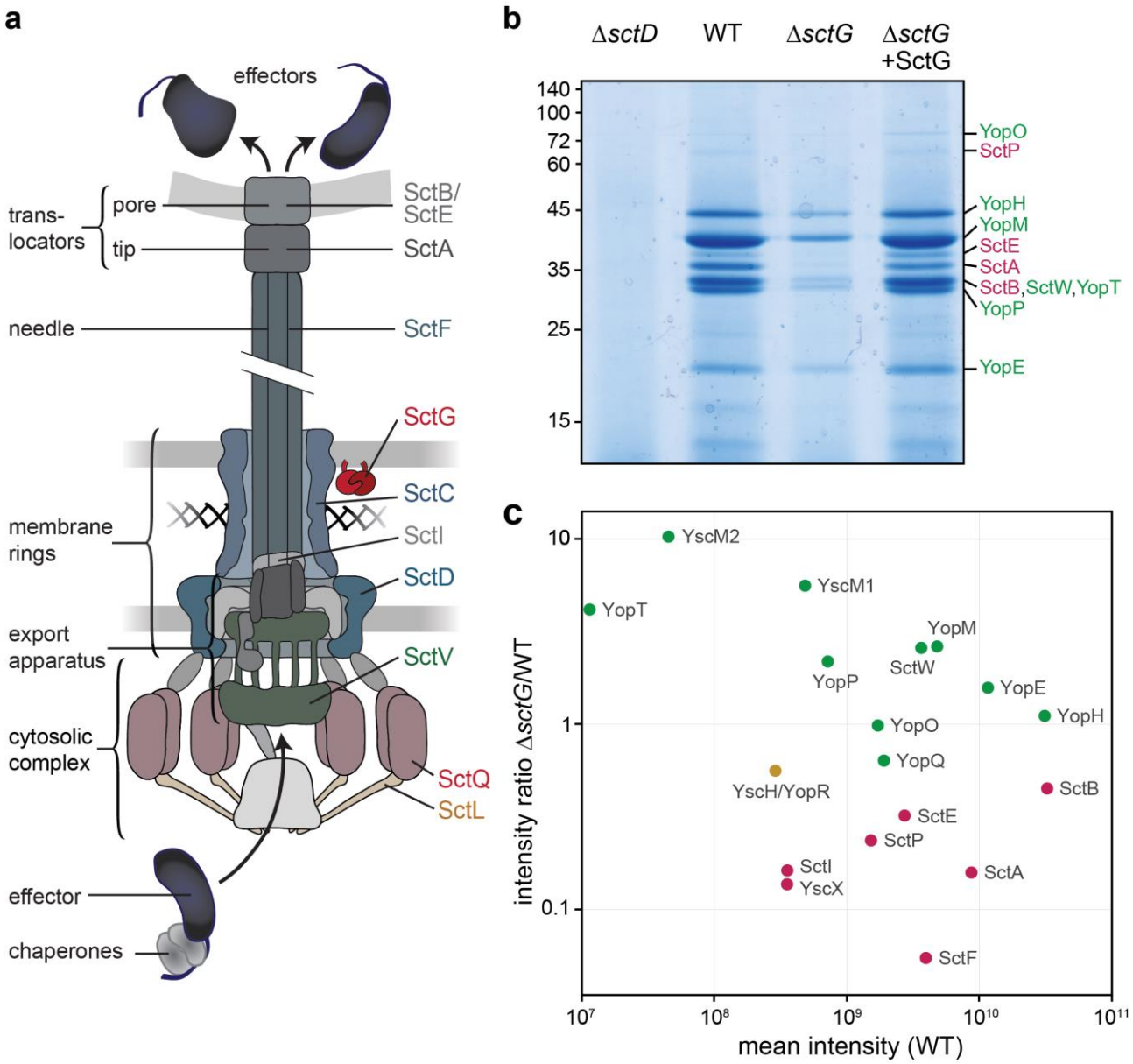

Fig. 1 – SctG is required for the secretion of early export substrates, but not of effectors.

a) Schematic illustration of the injectisome (adapted from Diepold and Wagner, 2014). Main substructures indicated on the left; components analyzed in this study, including the pilotin SctG and the secretin SctC, are indicated on the right and shown in color. **b**) Secretion assay showing the export of native T3SS substrates into the culture supernatant in the listed strains (*n*=3). Left, molecular weight in kDa; right, assignment of exported proteins. **c**) Label-free mass spectrometry quantification of secreted proteins in *ΔsctG* and wild-type (WT), intensity ratio plotted against mean intensity (*n*=3). In b) and c), early/middle T3SS export substrates are marked in magenta; late substrates (effectors) are marked in green; substrate with unknown time point of export marked in yellow.

135 **Table 1 – Influence of SctG on T3SS secretion substrates**

136 Label-free quantitative mass spectrometry of known T3SS substrates in the culture supernatant of
137 different strains, as indicated. Magenta shade, early and middle substrates; green shade, late substrates;
138 yellow shade, unknown. # pept., number of total detected peptides. Hits sorted by ratio of
139 *ΔsctG*/wild-type (WT). *n*=3, individual measurements listed in Table S2.

140

T3SS substrate	# pept.	Intensity ratio *ΔsctG* / WT	Mean intensity		
			WT	*ΔsctG*	*ΔsctC*
Needle component SctF	7	0.0547	3.95E+09	2.16E+08	1.65E+07
Early substrate / regulator YscX	4	0.1366	3.55E+08	4.85E+07	8.80E+06
Tip protein SctA (LcrV)	24	0.1580	8.72E+09	1.38E+09	1.07E+08
Rod / washer protein SctI	3	0.1621	3.56E+08	5.78E+07	2.07E+07
Needle length regulator / ruler SctP	23	0.2359	1.53E+09	3.60E+08	4.84E+07
Translocator SctE (YopB)	19	0.3213	2.73E+09	8.77E+08	3.44E+08
Translocator SctB (YopD)	46	0.4502	3.26E+10	1.47E+10	9.06E+08
Secreted protein YscH/YopR	4	0.5604	2.90E+08	1.62E+08	1.15E+07
Effector YopQ	16	0.6357	1.90E+09	1.21E+09	6.51E+06
Effector YopO	37	0.9833	1.72E+09	1.69E+09	6.58E+07
Effector YopH	64	1.1095	3.11E+10	3.45E+10	1.23E+09
Effector YopE	10	1.5746	1.16E+10	1.82E+10	2.67E+09
Effector YopP	25	2.1810	7.21E+08	1.57E+09	5.24E+06
Gatekeeper SctW (YopN)	17	2.5811	3.65E+09	9.42E+09	3.18E+07
Effector YopM	6	2.6303	4.81E+09	1.26E+10	7.99E+07
Effector YopT	7	4.1605	1.15E+07	4.77E+07	1.28E+07
Regulator YscM1	12	5.5968	4.84E+08	2.71E+09	9.81E+06
Regulator YscM2	7	10.2833	4.52E+07	4.65E+08	5.43E+06

141

142

143 **The pilotin is essential for stable localization of the export apparatus and the cytosolic**
144 **T3SS components, but few needles can form in its absence**

145 We next investigated the specific role of the pilotin in the assembly of the injectisome, which may
146 provide a clue to its function. To this aim, we deleted *sctG* in strains expressing fluorescently labeled
147 variants of the secretin (SctC-mCherry) [28], the large export apparatus component (SctV-EGFP)
148 [29], the cytosolic sorting platform component SctL (mCherry-SctL) [43], and a strain expressing
149 $SctF_{S5C}$, a variant of the needle protein that can be labeled by maleimide dyes [44]. Except for $SctF_{S5C}$,
150 which is expressed from plasmid, all other labeled proteins are expressed from their native genetic
151 environment. As expected, fluorescence microscopy of the respective bacteria showed an

152 important role of SctG in the assembly of the secretin ring. Far from its usual assembly in >10 mostly
153 lateral foci in the wild-type background, SctC mostly localized in large, often polar clusters in the
154 absence of the pilotin (Fig. 2a, left, Dataset S1). These SctC foci mostly do not correspond to fully
155 assembled injectisomes: SctV foci were motile in the membrane in the absence of SctG, like in the
156 absence of the secretin SctC (Fig. 2b, Fig. S2a) [29]. Moreover, we found that the cytosolic
157 component SctL formed very few foci in the absence of SctG (Fig. 2, center; Dataset S1).
158 Nevertheless, a small subset of bacteria lacking SctG did display needles (Fig. 2, right; Dataset S1).
159 These needles, however, did not colocalize with the sorting platform protein SctL (Fig. S2b). *In trans*
160 complementation of SctG restored wild-type localization of all tested components (Fig. S3). Notably,
161 levels of SctG significantly lower than in the wild-type were already sufficient for complementation
162 of secretion and injectisome assembly (Fig. S3).

163 The results above indicate that SctG is essential for proper assembly and anchoring of all major
164 subcomplexes of the injectisome, but that a subset of cells forms mostly polar needles in its absence.
165 We therefore next analyzed SctG itself to figure out how it conveys its function.

166

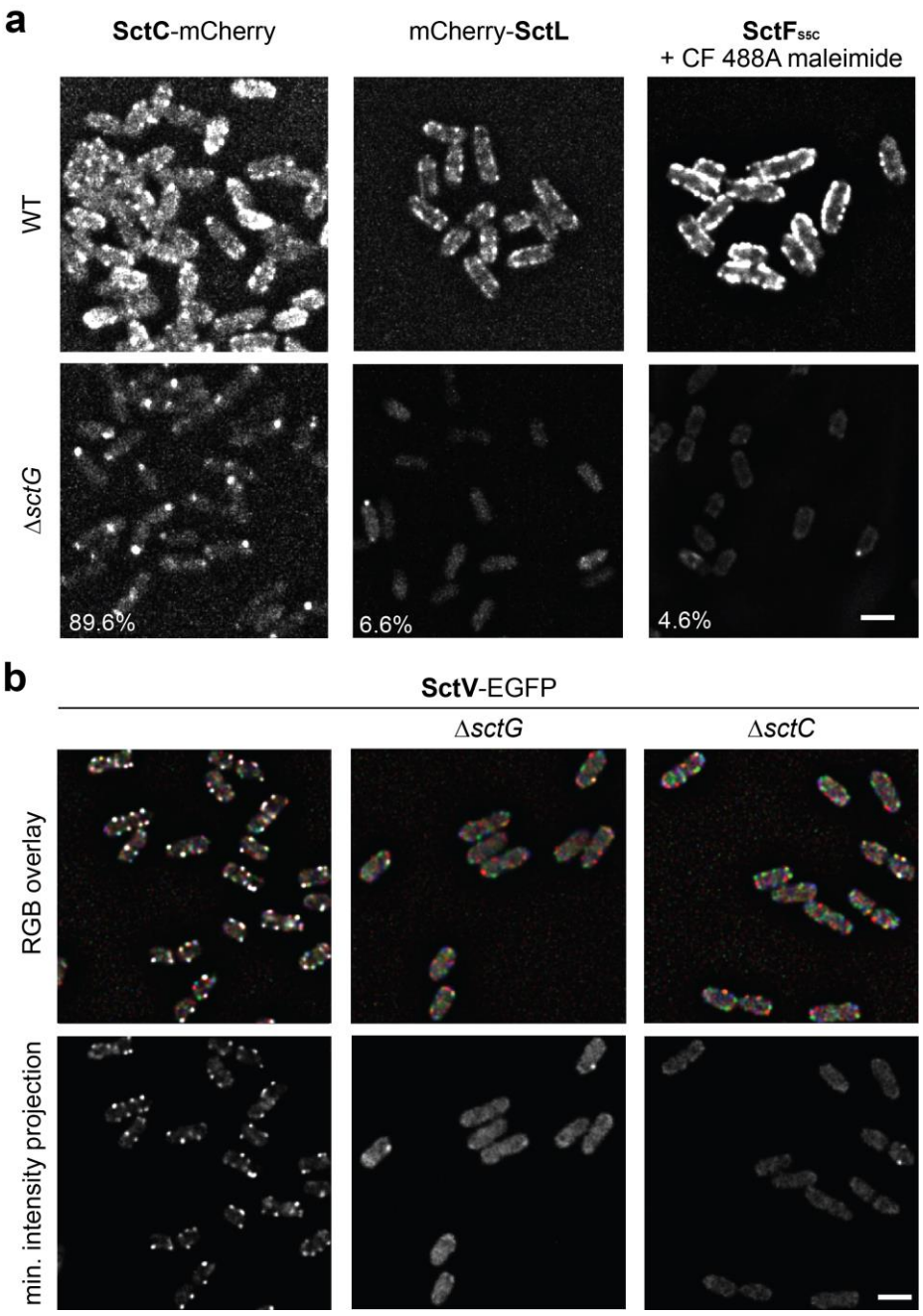

Fig. 2 – SctG is required for normal localization of SctC and stable assembly of the export apparatus and the sorting platform component SctL, but not fully essential for the formation of needles.

a) Fluorescence micrographs of *Y. enterocolitica* expressing the proteins indicated from their native location on the virulence plasmid (SctC-mCherry and mCherry-SctL) or *in trans* (SctF$_{S5C}$, stained with CF 488A maleimide stain) in an effector-less strain background. Top row displays native localization in wild-type (WT) background, bottom row localization in respective Δ*sctG* strain background. Scale bar, 2 µm. The fraction of bacteria with foci is listed for the respective Δ*sctG* strains. See Suppl. Dataset 1 for details. *n*=3-6. **b**) Red/green/blue (RGB) overlay and minimum intensity projection showing the movement of SctV-EGFP over time in the indicated effector-less strain backgrounds in live *Y. enterocolitica*. Red/green/blue channel: micrograph at t=0/15/30 s; white foci indicate stable protein localization, whereas colors indicate movement of foci over time. Minimum projection: micrographs at 0/15/30/45/60/75/90 s; foci indicate stable foci over this time period. *n*=3.

180

181 **Pilotin expression is controlled by temperature, similarly to structural T3SS components**

182 Pilotin proteins are abundant but not omnipresent in secretion systems. Despite their consistent
183 reported role for assembly of the highly conserved secretin, pilotins show low sequence
184 conservation (Fig. S4a). Accordingly, we found that even the pilotin from the closely related T3SS of
185 *P. aeruginosa* could not complement a *sctG* deletion in *Y. enterocolitica* (Fig. S4b).

186 Despite this low sequence conservation, pilotins have a conserved unique genetic location within
187 the virulence plasmids or genetic islands encoding the T3SS. While most other structural and
188 regulatory components of the injectisome are under the control of a main transcriptional regulator
189 (VirF in *Y. enterocolitica*, called LcrF in other *Yersinia* species), pilotins are located upstream of the
190 transcriptional regulator itself (genetic neighborhood analysis, Fig. 3a), indicating a specific role in
191 the T3SS with a potentially distinct expression pattern.

192 To unravel the expression kinetics, as well as the subcellular localization of SctG, we introduced a
193 *sctG-sfGFP* fusion in the native *sctG* locus on the *Y. enterocolitica* virulence plasmid by homologous
194 recombination [45]. The SctG-sfGFP fusion protein was stable and functional (Fig. S5). The
195 expression of SctG, VirF and, in consequence, other T3SS components was moderately increased
196 (1.5-2-fold) in the strain. Additionally, few non-T3SS proteins were affected by the fusions (Table
197 S3).

198 SctG-sfGFP was expressed at a level below the detection limit prior to the shift to 37°C, which
199 activates the VirF-dependent expression of other T3SS components. After the temperature shift,
200 SctG expression increased steadily over the next two hours (Fig. 3bc). Somewhat surprisingly, given
201 their different genetic regulation, the SctG-sfGFP expression profile did not differ significantly from
202 mCherry-SctD, a basal body protein labeled in the same strain (Fig. 3c).

203

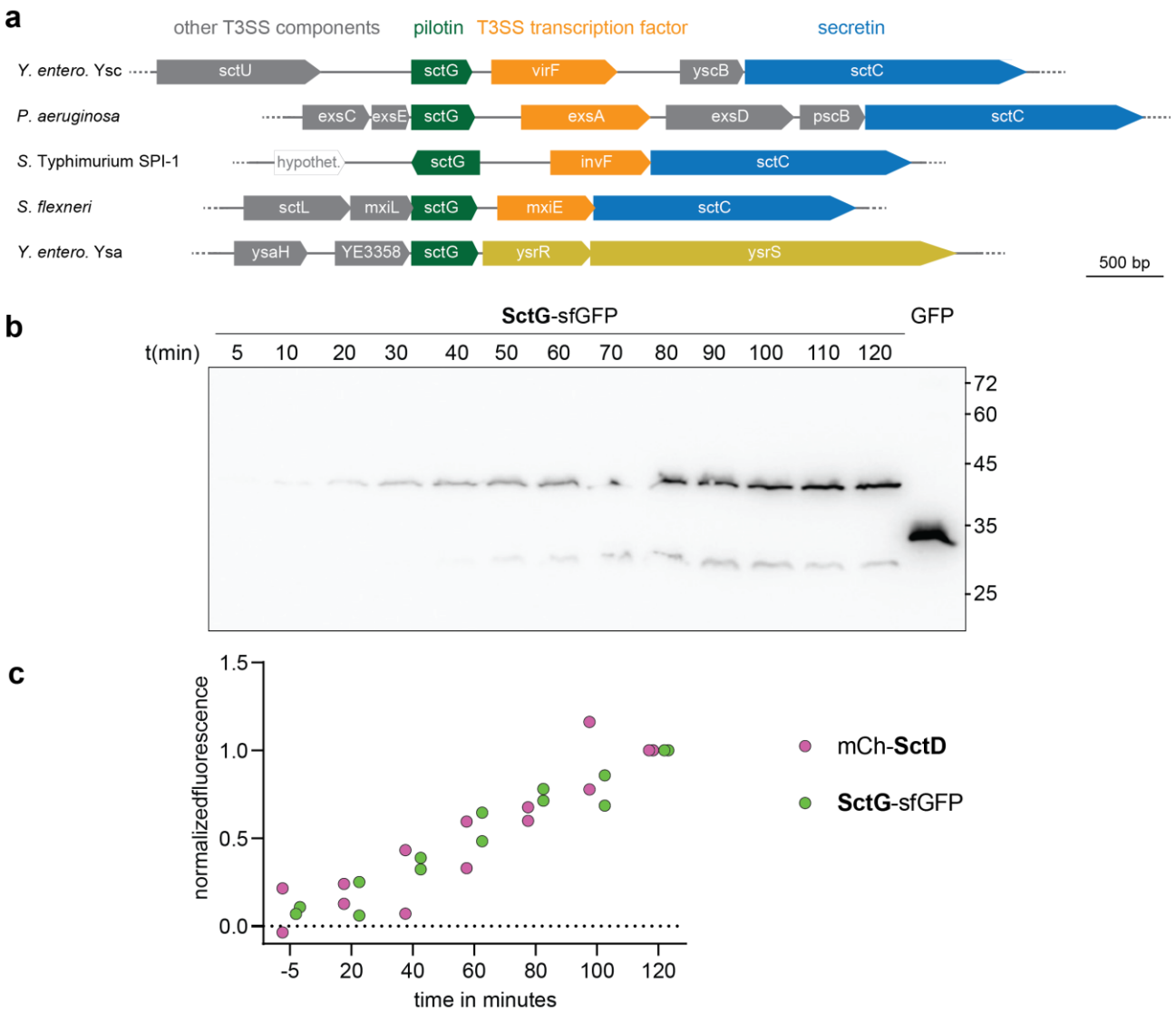

Fig. 3 – Despite its unique genetic location, SctG expression is regulated similar to other T3SS components.

a) Genetic neighborhood analysis of pilotin proteins (green) of the different T3SS indicated on the left side. Main T3SS transcription factors (orange), secretins (blue) and other T3SS components (gray) are indicated. The *ysrRS* phosphorelay system activating transcription of the Ysa system [46] is marked in yellow. **b**) Expression of SctG-sfGFP (expected molecular weight 42.2 kDa) over time under non-secreting conditions. Immunoblot using antibodies directed against GFP. Control: Expression of GFP from plasmid. Numbers indicate time in min relative to temperature shift to 37°C, which triggers the expression of T3SS components. Right, molecular weight in kDa. *n*=2. **c**) Expression of SctG-sfGFP and the IM ring component mCherry-SctD over time before and after temperature shift to 37°C in a double-labeled strain under non-secreting conditions. Quantification of fluorescence per bacterium, normalized by the respective 120 min value. Dots indicate individual biological replicates with a total of 52, 100, 128, 128, 217, 185, 143 bacteria (from left to right).

219 **Pilotins localize dynamically within the membrane and do not stably colocalize with other**
220 **injectisome components**

221 The functional SctG-sfGFP fusion allowed us to assay the cellular localization of SctG in live *Y.*
222 *enterocolitica*. Stable stoichiometric association with the secretin SctC would result in the formation
223 of membrane foci colocalizing with other injectisome components [28,43]. However, we detected a
224 disperse membrane localization of SctG-sfGFP which increased over time similar to overall protein
225 levels in the cell, in addition to cytosolic background fluorescence (Fig. 4a). While a certain clustering
226 of SctG-sfGFP in the membrane was visible, these clusters did not significantly colocalize with the
227 mCherry-labeled T3SS components SctC, SctD, or SctL, in contrast to the clear colocalization
228 observed for mCherry-SctD and EGFP-SctQ used as positive control (Fig. 4b, Fig. S6).

229

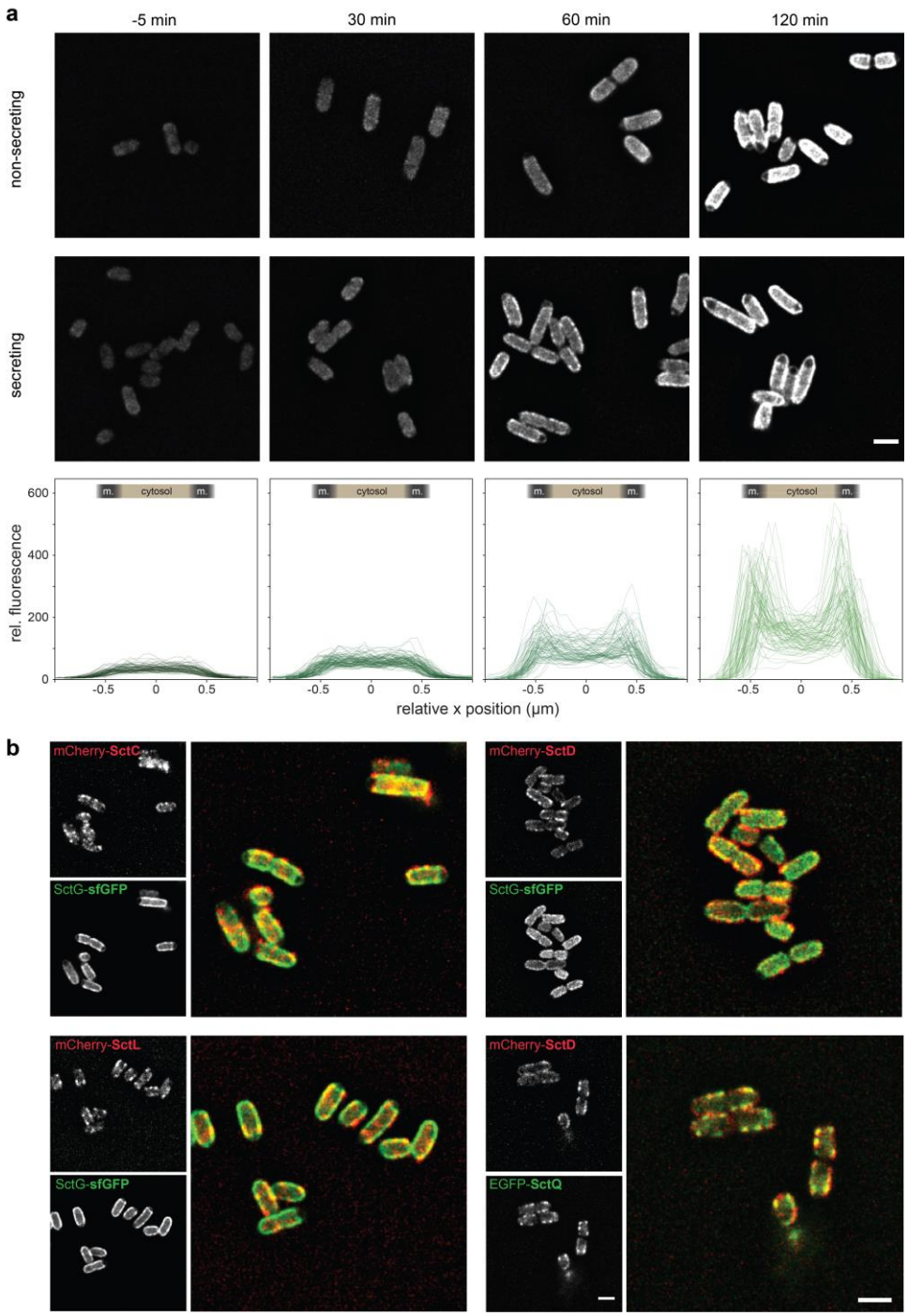

Fig. 4 – SctG predominantly localizes in the membrane, but does not significantly colocalize with other injectisome components.

a) Time course microscopy of SctG-sfGFP in *Y. enterocolitica* under non-secreting conditions. Time with reference to the temperature shift to 37°C. Bottom, intracellular localization of SctG-sfGFP at the respective time points. Line scans across single bacteria, approximate average positions of bacterial membranes (m., dark grey) and cytosol (beige) indicated. *n*=78, 90, 81, 90 cells (left to right) from three independent biological replicates. **b**) Colocalization of labeled T3SS components (all expressed from native genetic locus on virulence plasmid) in double-labeled strains as indicated, 120 min after temperature shift to 37°C. *n*=3, except for colocalization of mCherry-SctD and EGFP-SctQ, which was reported earlier [43] and included here as a positive control (*n*=1). Scale bars = 2 µm.

To analyze the mobility and cluster formation of SctG in more detail, we tracked SctG-sfGFP in individual bacteria. Still images and overlays (Fig. 5a), as well as movies (Suppl. Movie 1) showed that the localization of SctG and its clusters in the membrane strongly fluctuates, indicating diffusion within the membrane. We tested this hypothesis by fluorescence recovery after photobleaching (FRAP) and found that indeed, SctG-sfGFP is highly mobile within the membrane with an average half time of recovery at the bleached pole of 21.5 s (+/- 13.0s) (Fig. 5b).

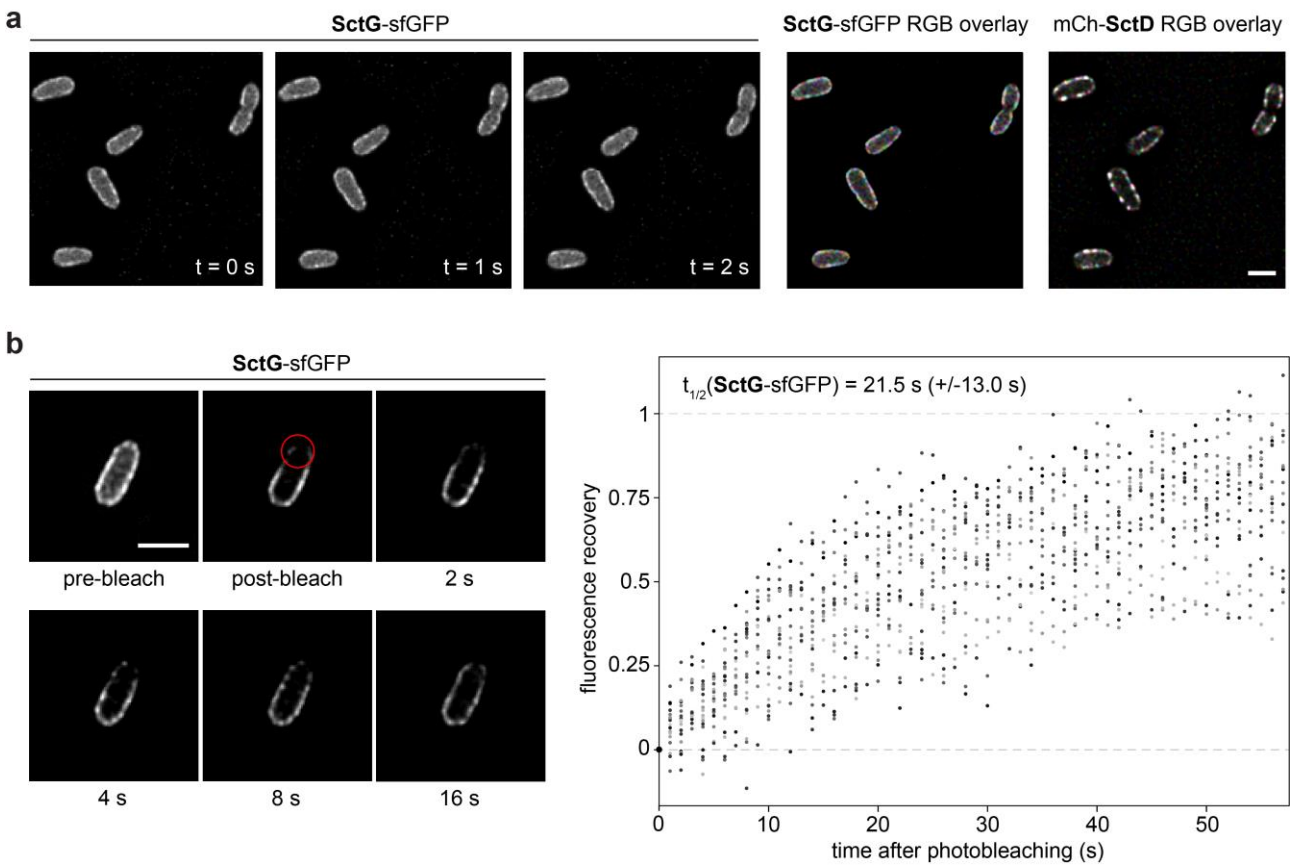

Fig. 5 – Pilotin proteins move dynamically within the membrane, forming transient patches.

Fluorescence microscopy of a strain expressing SctG-sfGFP and mCherry-SctD from their native genetic locations on the virulence plasmid. **a**) Left, single micrographs of SctG-sfGFP taken with 1 s difference. Right, red/green/blue (RGB) overlay of those micrographs for SctG-sfGFP and mCherry-SctD (mCh-SctD) (*n*=3). **b**) Fluorescence recovery after photobleaching for SctG-sfGFP. Left, representative individual micrographs before and at the indicated time points after the bleach event. Bleach spot indicated by red circle. Right, quantification of fluorescence recovery after photobleaching (*n*=21 cells from 3 independent experiments, displayed in different shades of grey). The recovery half-time $t_{1/2}$ was calculated for each individual recovery curve (see Material and Methods for details) and is displayed as average with standard deviation.

260

261 To investigate if SctG localization requires any other T3SS component or non-T3SS-related
262 *Y. enterocolitica* protein, SctG or SctG-sfGFP were expressed from plasmid in a *Y. enterocolitica*
263 strain cured of the virulence plasmid (pYV$^-$), as well as *Escherichia coli* Top10 (which has no T3SS)
264 (Fig. S7a). While SctG-sfGFP displayed a membrane localization in *Y. enterocolitica* pYV$^-$, similar to
265 its native localization, it localized predominantly to the cytosol in *E. coli* (Fig. S7ab). Notably,
266 expression of SctG negatively influenced the growth of *E. coli*. Strains expressing SctG or SctG-sfGFP
267 only grew to a low OD and microscopy experiments revealed severe lesions and plasmolysis in the
268 respective bacteria (Fig. S7ac), indicating that the pilotin localizes independently of other T3SS
269 components, but can be toxic upon ectopic expression. Taken together, SctG follows a similar
270 expression pattern as other VirF-controlled T3SS components despite its unique genetic location. It
271 localizes predominantly throughout the membrane, independently from other T3SS components,
272 and forms small transient patches.

273

274 **Proteome analysis and specific interactions of the pilotin to T3SS components and proteins**
275 **not directly linked to the T3SS**

276 The unexpected localization of SctG and the finding that amounts below the wild-type level are
277 sufficient for its function in injectisome assembly (Fig. S3) prompted us to consider additional roles
278 of SctG. To identify such roles in an unbiased way, we first compared the *Y. enterocolitica* proteome
279 in presence and absence of SctG under non-secreting conditions. In *ΔsctG*, the amount of the main
280 transcriptional activator VirF was reduced to about one third. Consequently, most other T3SS
281 components were also present at lower concentrations (Table S4). Absence of SctG had little impact
282 beyond the T3SS, with the notable exception of the OM protein OmpW, whose amount was reduced
283 by a factor of eight (Table S4).

284 To better understand the function of the pilotin, both with respect to the T3SS and other pathways,
285 we screened for interaction partners by co-immunoprecipitation with SctG-sfGFP, analyzed by label-
286 free mass spectrometry. As expected, SctG interacted with the secretin SctC, but also with other
287 T3SS components, most prominently the effector YopM and the large export apparatus protein SctV
288 (Fig. 6). Most other T3SS components were enriched to a lower degree (Fig. 6, Table S5).

289 Interestingly, a number of proteins not directly linked to the T3SS were enriched highly significantly.
290 Most prominently, the phosphoenolpyruvate (PEP)-dependent phosphotransferase system (PTS)
291 trehalose transporter subunit EIIBC (PTS-IIBC) consistently interacted very specifically with SctG (Fig.
292 6), despite low overall expression levels (Table S4). A closer look at the results also showed a
293 significant enrichment of several components of the Lol protein export pathway for the insertion of
294 lipoproteins into the OM, namely LolD and LolE, as well as other non-T3SS proteins, such as Lon
295 protease (termed endopeptidase La in *Y. enterocolitica*) and the prokaryotic tubulin homolog FtsZ,
296 a major player in cell division (Fig. 6, Table S5).

297

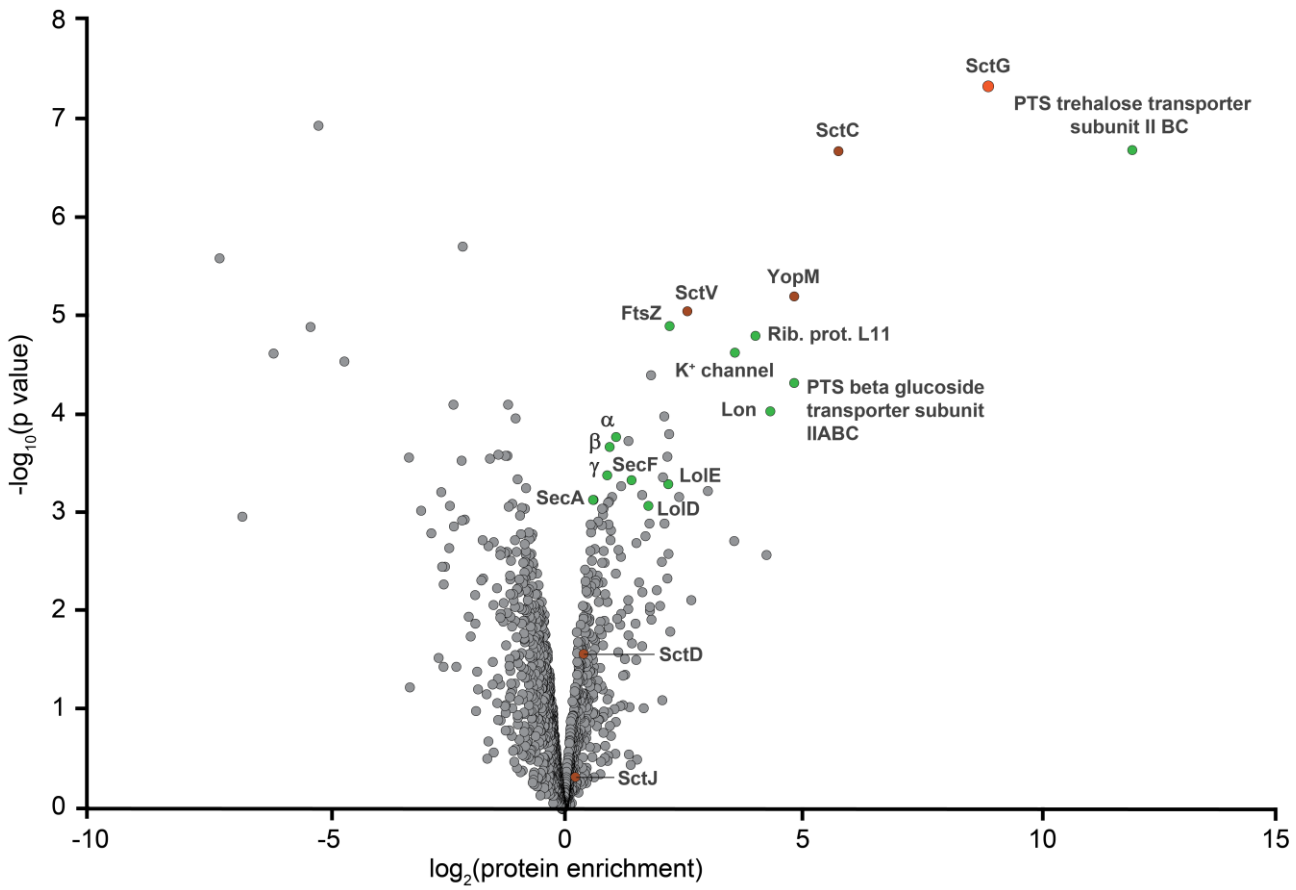

Fig. 6 – SctG interacts with T3SS components and additional non-T3SS proteins.

Co-immunoprecipitation experiments with SctG-sfGFP as bait, compared to an unlabeled control strain expressing sfGFP from plasmid at comparable levels. Interactors were quantified with label-free mass spectrometry (n=3). The bait protein SctG is marked in orange, other T3SS components in dark red, interactors discussed in the main text in green. Greek letters denote subunits of the F1 subcomplex of the ATP synthase. A full list of all interactors with p<0.001 and T3SS components can be found in Table S5.

Interestingly, PTS sugar transporters were shown to have a role in the regulation of the T3SS earlier [47]. We therefore constructed a clean *Δpts-IIBC* deletion mutant and tested its impact on assembly and function of the T3SS. PTS-IIBC was not required for assembly of injectisomes or effector secretion (Fig. 7a) and overexpression did not significantly impact T3SS localization or secretion itself (Fig. 7b).

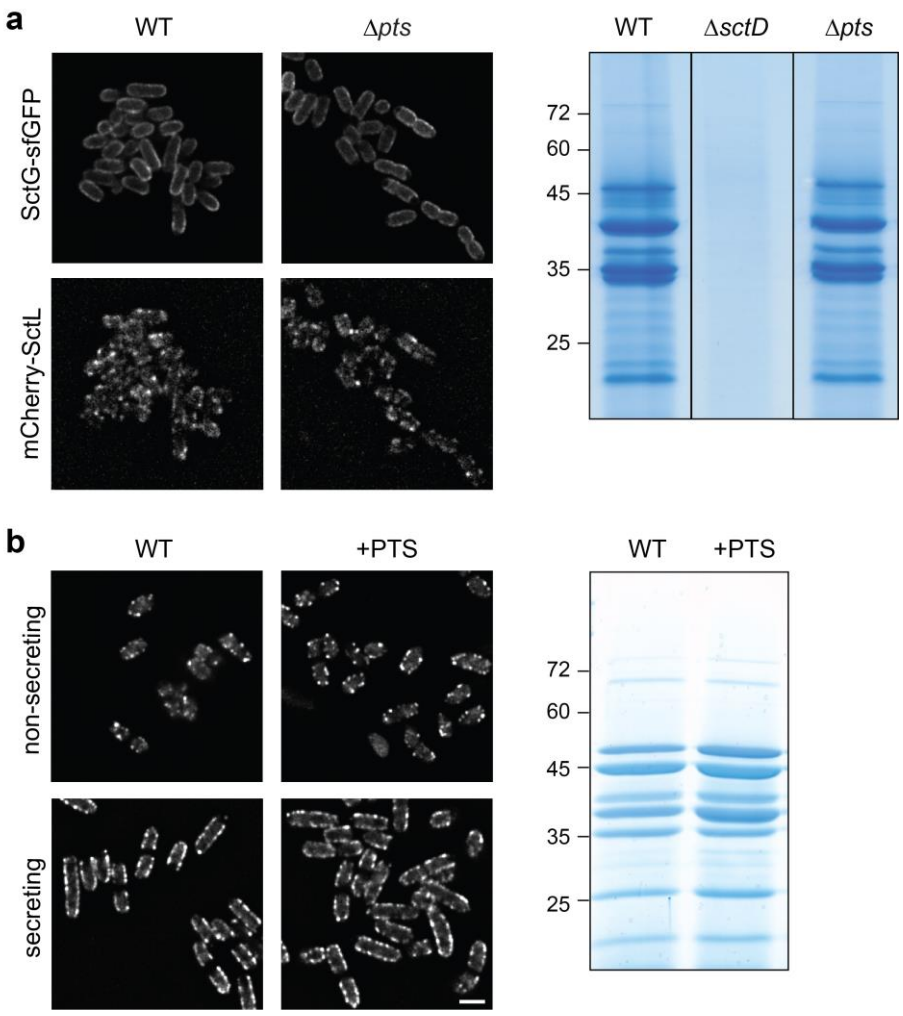

Fig. 7 – The SctG interactor PTS trehalose transporter subunit EIIBC does not affect assembly or function of the T3SS in rich medium.

a) Left: Micrographs of SctG-sfGFP and mCherry-SctL in double-labeled *Y. enterocolitica* strains otherwise wild-type (WT) or with a deletion of the PTS trehalose transporter subunit EIIBC (Δ*pts*). The experiment was performed under non-secreting conditions (*n*=3). Right: Secretion assay of the PTS trehalose transporter subunit EIIBC (Δ*pts*) deletion with WT and Δ*sctD* strains serving as positive and negative controls, under secreting conditions (*n*=2), molecular weight in kDa indicated. **b**) Left: Micrographs of EGFP-SctQ expressed from its native location on the virulence plasmid in *Y. enterocolitica* otherwise WT or overexpressing the PTS trehalose transporter subunit EIIBC (+PTS). Experiments performed under non-secreting and secreting conditions as indicated (*n*=3 each). Right: corresponding secretion assay, molecular weight in kDa indicated. Scale bar for all micrographs, 2 µm.

326 # Discussion

327 Pilotin proteins are conserved components of T3SS in many bacteria including most animal
328 pathogenic variants. They have a unique genetic location and a central role for the assembly of the
329 T3SS injectisome. However, little was known about their behavior and role beyond the assistance in
330 the proper localization and oligomerization of the secretin ring of the injectisome in the OM. In this
331 study, we confirm this role, but uncover an additional effect on T3SS export substrate selection.
332 Unexpectedly, we found that pilotins are mobile membrane components which may link the T3SS
333 to other cellular pathways, including sugar metabolism.

334 **Pilotins differentially affect major steps in T3SS assembly**

335 Pilotins have long been known to assist the assembly of the SctC secretin ring in the OM [18–
336 22,24,25]. Our data confirm these reports: In the absence of the pilotin, secretins localized in large
337 foci at one of the bacterial poles (Fig. 2a). The localization of other T3SS components in absence of
338 SctG differed from that of the secretin: SctL, a component of the cytosolic sorting platform of the
339 T3SS, only formed single, mostly polar, foci. Similarly, we observed few, also mostly polar, needles
340 for a subset of bacteria. However, these needles and the sorting platform protein SctL did not
341 colocalize (Fig. 2a, Fig. S2b), indicating an absence of stably assembled injectisomes. Consistent this,
342 the nonameric large export apparatus component SctV [48] assembled, but moved within the
343 membrane in the absence of SctG (Fig. 2b, Fig. S2a), indicating a lack of anchoring by the ring-
344 forming SctCDJ proteins [29]. Since all cytosolic T3SS components, including SctL, are required for
345 protein export under normal conditions, we speculate that transient interactions of SctL and the
346 other cytosolic T3SS components with basal body components at the poles might allow the limited
347 export of the needle subunit, which would then stay stably associated with the bacteria despite the
348 disassembly of the cytosolic sorting platform. In agreement with this hypothesis, we had found
349 earlier that the cytosolic T3SS sorting platform components do exchange between the injectisome-
350 bound sorting platform and a cytosolic pool [43,49] and that the sorting platform components
351 temporarily dissociate from the remaining injectisomes under certain conditions, such as low
352 external pH [50]. The presence of a low number of needles had previously been reported for the
353 closely related *P. aeruginosa* T3SS [19]. Notably, the fraction of bacteria with associated needles
354 and the overall secretion efficiency of the pilotin deletion showed an unusually high variation
355 between individual replication experiments, suggesting an influence of external factors. However,
356 despite our best efforts, we were unable to identify these factors.

357 **Role of pilotins in T3SS substrate specificity**

358 Analysis of the T3SS secretome by SDS-PAGE and quantitative mass spectrometry revealed a specific
359 effect of the presence of the pilotin on export of the so-called early substrates, required for
360 formation of the needle and its tip structure (Fig. 1, Table 1). Notably, while deletion or
361 modifications of *sctG* have an effect on the expression of VirF and its targets (Table S3, 4), most
362 likely due to an influence on the formation of hairpin structures in the *sctG-virF* mRNA that regulate
363 VirF transcription as part of the thermoregulation of T3SS expression [42,51], the role of SctG in
364 secretion substrate is independent from VirF levels (Fig. S1b). What could then be the reason for
365 the striking change of substrate specificity in absence of the pilotin, where early export substrate
366 are much more strongly affected by the absence of SctG than the late substrates, the virulence
367 effectors? Similar phenotypes had been found, although not always explicitly noted, in earlier
368 studies in *Y. enterocolitica* [15,25] and *P. aeruginosa* [19]. Taking into account the limited, probably
369 transient interaction of the pilotin with the secretin that we observed, it is tempting to speculate
370 that presence of the pilotin at the injectisome favors the secretion of early substrates. Subsequent
371 dissociation of the pilotin would then contribute to a switch in export cargo specificity towards the
372 effectors. The specific (albeit not necessarily direct) interaction of SctG with the large export
373 apparatus component SctV (Fig. 6), which is a key player in substrate selection [52–54], supports
374 this hypothesis.

375 Alternative explanations for the change in export substrate specificity might be (i) the polar
376 localization of the secretin (and consequently the hypothetical transient T3SS), which might change
377 the accessibility for certain substrates, or (ii) a two-step export pathway, with a first transport step
378 across the IM, facilitated by the T3SS export apparatus (which is assembled, albeit not anchored in
379 the peptidoglycan, in the absence of the pilotin (Fig. 2b)) and a subsequent export step across the
380 OM, facilitated by the secretin (without which no export is observed (Fig. S1)). The two-step
381 transport might prevent the export of early substrates, many of which polymerize outside the
382 cytosol. Alternatively, (iii) strains lacking the pilotin might be able to provide less energy due to the
383 missing link to the PTS sugar transporters or membrane stress as a consequence of secretin
384 misassembly. If effector export is less energy costly than the export of early substrates, this might
385 explain the observed bias in export in absence of SctG. However, in the absence of direct evidence
386 for these alternative explanations, we consider a direct influence of SctG on the substrate specificity
387 through interactions with other T3SS components to be the most likely explanation.

388 Substrate specificity switching is a central, but incompletely understood, feature type III secretion.
389 Our data suggest that pilotin proteins play a key role in this process, together with the export
390 apparatus components SctV and SctU [55], the gatekeeper complex [56,57] and the sorting platform
391 [58]. If and how the interaction of the pilotin with the effector YopM (Fig. 6) contributes to this
392 process is unclear at the moment.

393 Additional interactions of the pilotin after its dissociation from the injectisome and 394 possible functions

395 An unexpected finding of our study was that pilotin concentrations significantly below wild-type
396 levels are sufficient to restore normal T3SS assembly and function (Fig. S3). Although it is one of the
397 few T3SS machinery components encoded outside the VirF-regulated operons, native SctG
398 expression develops very similarly to other T3SS components (Fig. 3), consistent with the co-
399 transcription of *sctG* and *virF* in one operon [42]. However, the findings that low pilotin levels
400 already were sufficient for injectisome assembly and secretion and that SctG does not significantly
401 colocalize with other T3SS components (Fig. 4), but is highly mobile in the bacterial membrane (Fig.
402 5) suggests that the pilotin might have additional functions beyond its role in secretin assembly,
403 possibly after its release from the secretin. We therefore screened for additional interactors of SctG
404 by co-immunoprecipitation. Notably, while the pilotin mostly fractionates with the OM in
405 membrane preparations [18,25,59], many of the proteins found to interact with the labeled pilotin
406 in the co-immunoprecipitation assay are integral IM proteins or IM-associated proteins. The used
407 SctG-sfGFP fusion is expressed from its native genetic location, supports native secretion (Fig. S5),
408 and interacts with both known interactors, the secretin SctC and proteins of the Lol pathway, in our
409 assays (Fig. 6). Despite these indications for correct localization and interactions, it is possible that
410 transport of the fusion protein to the OM is impaired and that this at least enhances the fraction of
411 time the pilotin can contact these IM(-associated) proteins. Alternatively, the interactions may be
412 caused by natively soluble pilotin proteins, possibly bound to other proteins such as LolB [30,31].
413 Finally, the N-terminal lipid anchor of the pilotin might be removed after assembly of the secretin
414 ring or the injectisome, which would render the protein soluble [25] in the periplasm.

415 The most striking finding of the interaction studies was the highly specific enrichment of several PTS
416 sugar transporter subunits, most significantly the membrane-bound trehalose transporter subunit
417 EIIBC (Fig. 6, Table S5). PTS systems are used for sugar uptake in many bacteria. They create a
418 concentration gradient by transferring the PEP phosphoryl group onto the incoming sugar via

419 several intermediate phosphate carriers. The EIIC subunit, which can be fused to the EIIB subunit,
420 serves as channel in the IM. While many bacteria express several PTS transporters, PTS are often
421 unspecific and redundant [60]. Notably, PTS were repeatedly found to act as carbohydrate sensors
422 that control bacterial metabolism in response to the environment [61]. Transporters sensing host-
423 specific compounds can regulate expression and activity of virulence systems [62], indicating that
424 SctG and its main interactor, the PTS trehalose transporter subunit EIIBC, might serve to modulate
425 T3SS function according to the bacterial environment. The fact that so far, no pilotin homologs were
426 found in plant pathogens [3] is consistent with this hypothesis. Indeed, PTS systems were repeatedly
427 associated with bacterial virulence (reviewed in [60,63]): amongst others, presence of the PTS
428 glucose transporter subunit EIIBC conferred a competitive advantage to *Y. pestis* in serum-like
429 medium [64], a *Vibrio cholerae* PTS system was found to modulate virulence gene expression [65],
430 and *Salmonella* Typhimurium lacking a PTS EI subunit showed a nearly 1000-fold increase in LD_{50}
431 [66]. Specifically a PTS trehalose transporter system induces hypervirulence in *Clostridium difficile*
432 [67]. Notably, the PTS glucose transporter EIIA subunit directly interacts with cytosolic components
433 of the *Salmonella* SPI-2 T3SS and activates type III secretion [47]. Overall, the two most likely links
434 between PTS sugar transporters and virulence appear to be energy provision and/or host sensing.
435 Both possibilities are consistent with the lack of a phenotype of the *pts-IIbc* deletion in our
436 experiments (which were performed in rich medium in the absence of host cells, Fig. 7); however,
437 further experiments are required to describe the link in more detail.

438 Other significant interaction partners of the pilotin outside the T3SS are FtsZ, a prokaryotic tubulin
439 homolog with a key role in cell division, the protease Lon, components of the ATP synthase (subunits
440 α, β, γ), the Sec export pathway (SecF/A), and LolD/E, two components of the ABC transporter of
441 the Lol lipoprotein export pathway in the IM. FtsZ is an interesting interactor, as it might play a role
442 in the long-known, but still incompletely understood link between T3SS activity and cell growth and
443 division (actively secreting bacteria of many species cease growth and division and are often bigger
444 than T3SS-deficient or non-secreting bacteria [44,68–70]). Since to our knowledge, this is the first
445 time that a T3SS component was found to be associated with bacterial cytoskeleton proteins, this
446 might indicate an involvement of SctG in the non-random localization of T3SS around the cell
447 [12,13]. The Lon protease degrades unfolded or misfolded proteins, especially under stress
448 conditions [71], but can also have more specific roles in metabolism, cell cycle control and virulence
449 through proteolysis of specific regulatory proteins [72,73]. While it cannot be ruled out that the
450 specific interaction of SctG-sfGFP with Lon denotes degradation of partially misfolded SctG-sfGFP,

451 Lon proteases have been shown to influence T3SS activity, both positively via degradation of
452 histone-like proteins like *Yersinia* YmoA that suppress the transcription of T3SS components [74–
453 77] and negatively, most likely by directly degrading key components of the T3SS, mainly in plant
454 pathogens [78–81]. The presence of three components of the IM ATP synthase amongst the less
455 than forty specific interactors of the pilotin protein is remarkable and, in combination with the
456 strong interaction with the PTS sugar transporter, suggests a link with the bacterial energy
457 metabolism. While such a link is more than conceivable, given the high energy expense of type III
458 secretion [82], its details are unclear at the moment. As lipoproteins in the OM, pilotins are expected
459 to interact with components of both the Sec and the Lol pathway [30,32,83]. While most models
460 emphasize the interaction with LolA and LolB in the periplasm and OM, respectively, we detected
461 strong binding to LolD and LolE in the IM (Fig. 6, Table S5), but no significant binding to LolA or B. Of
462 the two models proposed for the role of pilotins in the assembly of the secretin ring by Majewski
463 and colleagues [31], our data therefore supports the second model where the pilotin is released
464 from LolB before interacting with the secretin.

465 Taken together, our data indicate that, besides their function in the assembly of the secretin ring of
466 the T3SS, pilotin proteins have additional roles linked to type III secretion. In their absence, assembly
467 of all T3SS subcomplexes and specifically the export of early secretion substrates is strongly
468 impeded, while effectors are exported efficiently. Pilotin protein interact with components of the
469 T3SS, most prominently the secretin SctC and the large export apparatus component SctV, but are
470 mobile in the bacterial membrane and do not stay attached to or even significantly colocalize with
471 the injectisome. In line with these findings, the pilotin also interacted with other cell wall-associated
472 proteins such as a PTS sugar transporter subunit.

473 A potential model integrating these findings is that during injectisome assembly, SctG interacts with
474 SctC, facilitates its oligomerization in the OM, and the formation of needles. At a later time point,
475 SctG dissociates from the fully assembled injectisome, which then favors the export of effectors
476 upon activation of the T3SS. The pilotin is mobile at this stage and may additionally support this
477 function by interacting with other partners, including PTS sugar transporters, which could provide
478 the necessary energy for secretion. Challenging this model in future studies may therefore lead to a
479 better understanding of the energy provision for the T3SS and its link to sugar import.

480

481 # Material and methods

482 ## Bacterial strain generation and genetic constructs

483 A list of strains and plasmids used in this study can be found in Supplementary Table 6. All *Y.*
484 *enterocolitica* strains used in this study are based on the *Y. enterocolitica* wild-type strain MRS40 or
485 the strain IML421asd (ΔHOPEMTasd). In IML421asd all major virulence effector proteins
486 (YopH,O,P,E,M,T) are absent. Furthermore, this strain harbors a deletion of the aspartate-beta-
487 semialdehyde dehydrogenase gene which renders the strain auxotrophic for diaminopimelic acid
488 (DAP), making it suitable for work in an biosafety class 1 environment [84].

489 ## Bacterial cultivation, secretion assays and protein analysis

490 *Y. enterocolitica* day cultures were inoculated from fresh stationary overnight cultures
491 supplemented with the relevant antibiotics and DAP (80 mg/ml), where required, to an OD_{600} of
492 0.15 for secreting and 0.12 for non-secreting conditions, respectively. As growth medium, BHI (brain
493 heart infusion broth) supplemented with nalidixic acid (35 mg/ml), DAP (80 mg/ml) where required,
494 glycerol (0.4%) and $MgCl_2$ (20 mM) was used. Where required, ampicillin was added (0.2 mg/ml) to
495 select for the maintenance of expression plasmids. For secreting conditions, 5 mM EGTA were
496 added; for non-secreting conditions, 5 mM $CaCl_2$ were added to the pre-warmed (approx. 55°C)
497 medium, which was filtered through a 0.45 µm filter before the addition of other supplements and
498 cooled down to ambient temperature for the experiments. After inoculation, day cultures were
499 incubated at 28°C for 90 min to reach exponential growth phase. Expression of the *yop* regulon was
500 then induced by a rapid temperature shift to 37°C in a water bath. Where indicated, protein
501 expression from plasmid (derivates of pBAD-His/B (Invitrogen) in all cases except expression of VirF
502 from pCL5 [85]) was induced at this point by the addition of 0.02–1.0% L-arabinose as indicated in
503 the respective experiments.

504 For protein secretion assays and analysis of total cellular proteins, bacteria were incubated for 2-3
505 h at 37°C, as indicated. 2 ml of the culture were collected at 21,000 *g* for 10 min. The supernatant
506 was removed from the total cell pellet and proteins were precipitated by addition of a final
507 concentration of 10% trichloroacetic acid (TCA) and incubation at 4°C for 1–8 h. Precipitated
508 proteins were collected by centrifugation for 15 min at 21,000 *g* and 4°C, the pellet was washed
509 once with 1 ml ice cold acetone and subsequently resuspended and normalized in SDS-PAGE loading
510 buffer. Total cellular protein samples were normalized to 0.3 OD units (ODu, 1 ODu is equivalent to

511 1 ml of culture at on OD_{600} of 1, corresponding to approximately 5 x 10^8 *Y. enterocolitica*) and
512 supernatant samples to 0.6 ODu. Before loading, samples were incubated for 5 min at 99°C.
513 Separation was performed on 11%, 15% or gradient 12–20% SDS-PAGE gels, using BlueClassic
514 Prestained Marker (Jena Biosciences) as a size standard. For visualization, the SDS-PAGE gels were
515 stained with InstantBlue (Expedeon). For immunoblots, the separated proteins were transferred
516 from the SDS-PAGE gel onto a nitrocellulose membrane. Primary mouse antibodies against GFP
517 (1:4000) (ThermoFisher Proteintech 66002-1-lg, 1:4000) were used in combination with secondary
518 anti-mouse antibodies conjugated to horseradish peroxidase (Sigma A8275, 1:5000). For
519 visualization, ECL chemiluminescence substrate (Pierce) was used in a LAS-4000 Luminescence
520 Image Analyzer.

521 **Fluorescence microscopy**

522 For fluorescence microscopy, bacteria were treated as described above. After 2–3 h at 37°C, 400 µl
523 of bacterial culture were collected by centrifugation (2400 × g, 2 min) and reconstituted in 200 µl
524 minimal medium (100 mM 2-[4-(2-Hydroxyethyl)piperazin-1-yl]ethane-1-sulfonic acid (HEPES) pH
525 7.2, 5 mM $(NH_4)_2SO_4$, 100 mM NaCl, 20 mM sodium glutamate, 10 mM $MgCl_2$, 5 mM K_2SO_4, 50 mM
526 2-(N-morpholino)ethanesulfonic acid (MES), 50 mM glycine). 2 µl of resuspension were spotted on
527 agarose pads (1.5% low melting agarose (Sigma-Aldrich) in minimal medium) in glass depression
528 slides (Marienfeld). Where required, agarose pads and media were supplemented with 80 mg/ml
529 DAP for ΔHOPEMTasd-based strains, 5 mM $CaCl_2$ for non-secreting conditions, or 5 mM EGTA for
530 secreting conditions.

531 Microscopy was performed on a Deltavision Elite Optical Sectioning Microscope equipped with an
532 UPlanSApo 100×/1.40 oil objective (Olympus), using an Evolve EMCCD camera (Photometrics).
533 Where applicable, the prepared samples were illuminated first in the mCherry = 0.4 s with a mCherry
534 filter set and afterwards in GFP = 0.2 sec with a GFP filter set. Depending on the experiment, z stacks
535 with 1-15 slices (Δz = 0.15 µm) per fluorescence channel were acquired. The acquired micrographs
536 where subsequently deconvolved using softWoRx 7.0.0 (standard "conservative" settings). Images
537 were further processed with FIJI (ImageJ 1.51f/1.52i/1.52n) [86]. Where necessary, a drift correction
538 with the StackReg Plugin [87] was performed. Fluorescence quantification was performed in FIJI. For
539 presentation of micrographs in a figure, representative fields of view were selected, and brightness
540 and contrast of the micrographs was adjusted identically within the compared image sets.

541 **Maleimide-based needle (SctF) staining.**

542 Maleimide-based staining to visualize the injectisome needles was performed as described in [50].
543 Briefly, expression of $SctF_{S5C}$ from the pBAD-His/B plasmid was induced by addition of 1.0% L-
544 arabinose at the time of the temperature shift in strains expressing the native SctF at the same time.
545 After 2-3 h, bacteria were collected and resuspended in 0.2 volumes of minimal medium
546 supplemented with 5 µM of CF 488A maleimide dye (Sigma-Aldrich, USA) at 37 °C for 5 min. After
547 staining, cells were washed once with 1500 µl of minimal medium and resuspended in 200 µl of
548 minimal medium. 2 µl of bacterial suspension were spotted on 1.5% agarose pads in minimal
549 medium and visualized under the microscope as described above.

550 **Classification and quantification of fluorescent foci**

551 To determine the number of stable YscV-EGFP foci, seven micrographs were taken in 15 s intervals
552 and the minimal intensity for each location was determined from the deconvoluted micrographs.
553 Foci were then identified in FIJI using an intensity threshold of 700 (determined in images of the
554 wild-type background strain) and the "analyze particles" function with a minimal size of 4 pixels and
555 a particle circularity of 0.5-1.0. To evaluate the fraction of bacteria with foci for SctC-mCherry,
556 mCherry-SctL and $SctF_{S5C}$ in the absence of SctG, foci were manually identified and classified as
557 polar, subpolar and lateral based on their subcellular localization in deconvoluted micrographs. In
558 case a cell displayed multiple foci in different localization classes, bacteria were classified as
559 containing a lateral, subpolar, polar focus in descending order (e.g. a bacterium with a lateral and a
560 polar focus was assigned "lateral"). The overall number of bacteria in a field of view was determined
561 by using the deep learning based network, DeepBacs [88], that was previously trained with
562 differential interferometry contrast (DIC) micrographs of *Y. enterocolitica*. The overall percentage
563 of cells with foci is displayed in the figure.

564 **Fluorescence distribution analysis**

565 For analysis of the fluorescence distribution across bacteria, line scan analysis was performed on
566 deconvoluted micrographs in FIJI. With the straight line freehand tool, measurements areas were
567 defined from one lateral membrane to the other at a 90° angle. Per condition, 3 fields of view with
568 18-30 cells were analyzed and the background was measured. The line scans were individually
569 corrected for background fluorescence, normalized (fluorescence fraction relative to overall
570 fluorescence over background) and centered at the position closest to center of the total
571 fluorescence over background.

572 **Fluorescence recovery after photobleaching (FRAP)**

573 Cells were grown in non-secreting medium as described above. Samples were taken after 3 h at
574 37°C. To minimize unnecessary bleaching, no z stacks were acquired. Three pre-bleach images were
575 acquired and locations near selected bacterial cell poles were photobleached by individual 30 ns
576 pulses of a 488 nm laser. Recovery of the bleached foci was followed by time-lapse microscopy.
577 Deconvolved micrographs were used for the fluorescence quantification.

578 The relative fluorescence of the bleached spot was calculated as follows:

579 $$\text{Relative flourescence} = \frac{(Intensity\ bleached\ cell\ pole - Intensity\ background)}{(Intensity\ total\ cell - Intensity\ background)}$$

580 The relative fluorescence was then normalized (average pre-bleach value set to 1; post-bleach value
581 set to 0) and an exponential recovery was fitted using the equation:

582 $$y = A(1 - e^{-bx})$$

583 where y stands for the relative fluorescence, x for the time, A for the overall ratio of fluorescence
584 recovery, and b for the inverse of the time constant $\tau_{1/2}$. For the fit, A was restricted to values
585 between 0.7 and 1.1. Each bleach curve was fitted individually, and fits with $R^2 < 0.7$ were excluded
586 from further analysis. The half-time of recovery was calculated from the time constant as follows:

587 $$t_{1/2} = \ln(2)\,\tau_{1/2}$$

588 **Proteome and secretome analysis by shotgun proteomics based mass spectrometry**

589 Strains were grown and prepared as described above. After 2.5 h at 37°, cultures were normalized
590 to an OD_{600} of 0.5 and 2 ml were harvested by centrifugation at 9,391 *g* for 2 min. Cell were washed
591 3 times with 1x phosphate buffered saline (PBS) (8 g/l NaCl, 0.2 g/l KCl, 1.78 g/l Na_2HPO_4*$2H_2O$, 0.24
592 g/l KH_2PO_4, pH 7.4). After washing, the cell pellet was resuspended in 300 µl lysis buffer (2% sodium
593 lauroyl sarcosinate (SLS), 100 mM ammonium bicarbonate (ABC)) and incubated at 90°C for 10 min.
594 Protein concentrations were measured using a BCA assay (Thermo Scientific) and following
595 reduction in 5 mM Tris(2-carboxyethyl) phosphin (TCEP, 15 min at 90 °C) and alkylation in 10 mM
596 iodoacetamid (30 min, 20°C in the dark), 50 µg protein was used for tryptic digestion (1 µg, Serva)
597 at 30°C overnight in presence of 0.5% SLS. After digestion, SLS was precipitated by adding a final
598 concentration of 1.5% trifluoroacetic acid (TFA).

599 Desalting of cleared peptide samples was performed in C18 solid phase extraction (SPE) cartridges
600 (Macherey-Nagel). First, cartridges were prepared by adding acetonitrile, followed by equilibration
601 using 0.1% TFA and loading of peptide samples. Cartridges were washed with buffer containing 5%
602 acetonitrile and 0.1% TFA, and finally eluted with 50% acetonitrile and 0.1% TFA into a fresh tube.
603 Eluted peptides were dried and reconstituted in 0.1% TFA for LC-MS analysis.

604 Purified peptides were analyzed by liquid chromatography-mass spectrometry (MS) carried out on
605 a Q-Exactive Plus instrument connected to an Ultimate 3000 rapid-separation liquid
606 chromatography (RSLC) nano instrument and a nanospray flex ion source (all Thermo Scientific).
607 Peptide separation was performed on a reverse-phase high-performance liquid chromatography
608 (HPLC) column (75 µm by 42 cm) packed in-house with C_{18} resin (2.4 µm; Dr. Maisch GmbH). The
609 peptides were first loaded onto a C18 precolumn (preconcentration set-up) and then eluted in
610 backflush mode with a gradient from 98 % solvent A (0.15 % formic acid) and 2 % solvent B (99.85
611 % acetonitrile, 0.15 % formic acid) to 25 % solvent B over 66 min, continued from 25 to 40 % of
612 solvent B up to 90 min. The flow rate was set to 300 nl/min. The data acquisition mode for label-
613 free quantification (LFQ) was set to obtain one high-resolution MS scan at a resolution of 70,000
614 (*m/z* 200) with scanning range from 375 to 1500 *m/z* followed by MS/MS scans of the 10 most
615 intense ions at a resolution of 17,500. To increase the efficiency of MS/MS shots, the charged state
616 screening modus was adjusted to exclude unassigned and singly charged ions. The dynamic
617 exclusion duration was set to 10 s. The ion accumulation time was set to 50 ms (both MS and
618 MS/MS). The automatic gain control (AGC) was set to 3×10^6 for MS survey scans and 1×10^5 for
619 MS/MS scans.

620 Due to an instrument upgrade, the QExactive Plus system was replaced by an Exploris 480 mass
621 spectrometer (Thermo Scientific). For total proteome analysis, purified peptides were analyzed
622 using identical LC settings, and the Exploris MS data acquisition settings were the following: one
623 high-resolution MS scan at a resolution of 60,000 (m/z 200) was obtained with scanning range from
624 350 to 1650 m/z followed by MS/MS scans of 2 sec cycle time at a resolution of 15,000. Charge state
625 inclusion was set between 2 and 6. The dynamic exclusion duration was set to 14 s. The ion
626 accumulation time was set to 25 ms for MS and AUTO for MS/MS. The automatic gain control (AGC)
627 was set to 300% for MS survey scans and 200% for MS/MS scans.

628 LFQ analysis was performed using MaxQuant [89] in standard settings using a *Y. enterolitica* protein
629 database containing proteins of the closely related *Y. enterocolitica* strain W22703 [90] and of the
630 pYVe227 virulence plasmid (GenBank entry AF102990.1). Statistical follow-up analysis of the

631 MaxQuant LFQ data was performed on an updated SafeQuant [91,92] R-script modified to routinely
632 process MaxQuant "protein groups" outputs. The missing value imputation was adapted from
633 Perseus [93] in default settings and implemented into the update SafeQuant script. Unless
634 otherwise indicated, proteins with ≥3 detected peptides and a *p* value ≤ 0.01 of the sample versus
635 the control using Student's t-test were considered as enriched and displayed in the tables. Intensity
636 values were shaded according to their value (blue for high intensity; transparent for low intensity)
637 for easier visualization.

638 For secretome analysis and quantification of secreted effectors in the supernatant, 5 ml BHI cultures
639 were grown under secreting conditions in 15 ml tubes as otherwise described before. After two
640 hours of incubation at 37°C, the medium was changed from BHI to minimal medium supplemented
641 with nalidixic acid (35 mg/ml), diaminopimelic acid (80 mg/ml) where required, glycerol (0.4%),
642 $MgCl_2$ (20 mM) and EGTA (5 mM). Next, bacteria were again incubated at 37°C shaking for one hour.
643 Samples were OD-normalized in a 2 ml volume, and bacteria were removed by centrifugation (10
644 min at 21,000 *g*, 4°C). In the next step, the supernatant was removed and precipitated with a final
645 concentration of 10% TCA for 1–8 h at 4°C; proteins were collected by centrifugation for 15 min at
646 21,000 *g* at 4°C and washed once with 1 ml ice cold acetone. A detailed description of the
647 experimental procedure is shown in [94]. The remaining pellet was resuspended in 300 µl lysis buffer
648 and incubated at 90°C for 10 min. Following reduction and alkylation (see above), proteins were
649 digested using 1 µg trypsin. All further steps including C18-SPE, LC-MS analysis and LFQ data analysis
650 were identical to the ones described above. The LC separating gradient length was reduced to 45
651 min due to lower sample complexity.

652 **Co-immunoprecipitation and shotgun proteomics**

653 For co-immunoprepitation, 100 ml of non-secreting culture medium were inoculated to an OD_{600} of
654 ~0.15 and treated as described above. After 2.5 h incubation at 37°C, the cultures were transferred
655 to 50 ml tubes and centrifuged at 2,000 *g* for 15 min at 4°C. Pellets were washed with 10 ml of 1x
656 PBS. The contents of two tubes were pooled and centrifuged at 2,000 *g* for 15 min at 4°C. The pellet
657 was resuspended in 2 ml HNN lysis buffer (50 mM HEPES pH 7.5, 150 mM NaCl, 50mM NaF, sterile
658 filtered; protease inhibitor (cOmplete Mini, EDTA free (Roche)) added before use), and incubated
659 for 30 min on a turning wheel at 4°C. Afterwards the bacteria were sonicated with 12 pulses à 30 s
660 in a Hielscher UP200ST ultrasonic homogenizer. The cells were again placed on a turning wheel for
661 30 min at 4°C and the sonification process and the subsequent incubation on a turning wheel were
662 repeated. Unbroken cells were removed by centrifugation (20,000 *g*, 20 min, 4°C). For affinity

purification, 10 µl of bead slurry (GFP-Trap Magnetic Agarose, Chromotek) were added to the lysate and incubated shaking for 1 h at 4°C on a turning wheel. Beads were washed with 500 µl HNN lysis buffer + 0.1% NP40, followed by seven consecutive washing steps with 700 µl 100 mM ABC. 200 µl of elution buffer (100 mM ABC, 1 µg trypsin per sample) were added to the beads and incubated for 45 min on a thermomixer at 30°C at 1200 rpm. Beads were separated and the supernatant was collected. Beads were washed twice using 80 µl of elution buffer 2 (1 M urea, 100 mM ABC, 5 mM TCEP), combined with the first eluate fraction and incubated o/n at 30°C to complete proteolysis. To monitor the experimental steps, samples for Western blot analysis were taken throughout the whole procedure. After digest, 10 mM iodoacetamid were added and the samples were incubated for 30 min in the dark. For desalting, C18 solid phase extraction cartridges samples were acidified and the procedure was carried out as described above. The samples were analyzed on a QExactive Plus mass spectrometer using a resolving LC gradient of 40 min. The analytical settings and data analysis steps including MaxQuant and SafeQuant are described above. Unless otherwise indicated, proteins with ≥3 detected peptides and a p value ≤ 0.001 of the sample versus the control using Student's t-test were considered as enriched and displayed in the tables.

Sequence analysis

For the analysis of the genetic environment of T3SS pilotin proteins from model organisms, the following GenBank sequences were used: AF102990.1 (*Yersinia enterocolitica* plasmid pYVe227, complete sequence), NC_002516.2 (*Pseudomonas aeruginosa* PAO1, complete genome reference sequence), NC_003197.2 (*Salmonella enterica* subsp. *enterica* serovar Typhimurium str. LT2, complete genome reference sequence), NC_004851.1 (*Shigella flexneri* 2a str. 301 plasmid pCP301, complete sequence), AM286415.1 (*Yersinia enterocolitica* subsp. *enterocolitica* 8081, complete genome). Multiple sequence alignment of the *sctG* and *sctC* genes of the same systems was performed using T-COFFEE 11.0 [95].

688 ## Acknowledgements

689 This work was supported by the Max Planck Society. The authors thank Christoph Spahn (Max Planck
690 Institute for Terrestrial Microbiology, Marburg, Germany) for fruitful discussions about microscopy
691 data analysis and his help with implementing the DeepBacs segmentation tool for *Y. enterocolitica.*

692

693 **Author contributions**

694 S.W. performed the majority of the experiments and data analysis and participated in study design
695 and writing of the manuscript. M.F. performed experiments, implemented methods and generated
696 key strains for this study. C.H., C.B. and K.L. assisted in experiments and strain generation. W.S., G.A.
697 T.G. from the Proteomics facility provided this technology and assisted in data evaluation and
698 statistical analysis. A.D. conceived and designed the study, performed data analysis and wrote the
699 manuscript.

700

701 **Competing interests**

702 The authors declare no competing interests.

703

704 # References

705 1. Galán JE, Wolf-Watz H. Protein delivery into eukaryotic cells by type III secretion machines.
706 Nature. 2006 Dec 1;444(7119):567–73.

707 2. Cornelis GR. The type III secretion injectisome. Nat Rev Microbiol. 2006 Oct 17;4(11):811–25.

708 3. Büttner D. Protein export according to schedule: architecture, assembly, and regulation of type
709 III secretion systems from plant- and animal-pathogenic bacteria. Microbiol Mol Biol Rev. 2012
710 Jun 1;76(2):262–310.

711 4. Burkinshaw BJ, Strynadka NC. Assembly and structure of the T3SS. Biochim Biophys Acta - Mol
712 Cell Res. 2014 Feb 7;1843(8):1648–93.

713 5. Wagner S, Grin I, Malmsheimer S, Singh N, Torres-Vargas CE, Westerhausen S. Bacterial type III
714 secretion systems: a complex device for the delivery of bacterial effector proteins into
715 eukaryotic host cells. FEMS Microbiol Lett. 2018 Aug 1;365(19).

716 6. Diepold A, Wagner S. Assembly of the bacterial type III secretion machinery. FEMS Microbiol
717 Rev. 2014 Jul 3;38(4):802–22.

718 7. Journet L, Agrain C, Broz P, Cornelis GR. The needle length of bacterial injectisomes is
719 determined by a molecular ruler. Science (80-). 2003 Dec 6;302(5651):1757–60.

720 8. Wee DH, Hughes KT. Molecular ruler determines needle length for the Salmonella Spi-1
721 injectisome. Proc Natl Acad Sci. 2015 Mar 16;112(13):4098–103.

722 9. Chakravortty D, Rohde M, Jäger L, Deiwick J, Hensel M. Formation of a novel surface structure
723 encoded by Salmonella Pathogenicity Island 2. EMBO J. 2005 Jun 1;24(11):2043–52.

724 10. Blocker AJ, Gounon P, Larquet E, Niebuhr K, Cabiaux V, Parsot C, et al. The tripartite type III
725 secreton of Shigella flexneri inserts IpaB and IpaC into host membranes. J Cell Biol. 1999 Nov
726 1;147(3):683–93.

727 11. Diepold A, Armitage JP. Type III secretion systems: the bacterial flagellum and the injectisome.
728 Philos Trans R Soc B Biol Sci. 2015 Oct 5;370(1679):20150020.

729 12. Kudryashev M, Diepold A, Amstutz M, Armitage JP, Stahlberg H, Cornelis GR. Yersinia
730 enterocolitica type III secretion injectisomes form regularly spaced clusters, which incorporate
731 new machines upon activation. Mol Microbiol. 2015 Dec 18;95(5):875–84.

732 13. Zhang Y, Lara-Tejero M, Bewersdorf J, Galán JE. Visualization and characterization of individual
733 type III protein secretion machines in live bacteria. Proc Natl Acad Sci U S A. 2017 Jun
734 6;114(23):6098–103.

735 14. Burgess JL, Case HB, Burgess RA, Dickenson NE. Dominant negative effects by inactive Spa47
736 mutants inhibit T3SS function and Shigella virulence. Cascales E, editor. PLoS One. 2020 Jan
737 24;15(1):e0228227.

738 15. Allaoui A, Scheen R, Lambert de Rouvroit C, Cornelis GR. VirG, a Yersinia enterocolitica
739 lipoprotein involved in Ca2+ dependency, is related to exsB of Pseudomonas aeruginosa. J
740 Bacteriol. 1995 Jul 31;177(15):4230–7.

741 16. Hardie KR, Lory S, Pugsley AP. Insertion of an outer membrane protein in Escherichia coli
742 requires a chaperone-like protein. EMBO J. 1996 Mar;15(5):978–88.

743 17. Koo J, Burrows LL, Lynne Howell P. Decoding the roles of pilotins and accessory proteins in
744 secretin escort services. FEMS Microbiol Lett. 2012 Mar 1;328(1):1–12.

745 18. Rau R, Darwin AJ. Identification of YsaP, the pilotin of the Yersinia enterocolitica Ysa type III

746 secretion system. J Bacteriol. 2015;197(17):2770–9.

747 19. Perdu C, Huber P, Bouillot S, Blocker AJ, Elsen S, Attree I, et al. ExsB is required for correct
748 assembly of Pseudomonas aeruginosa type III secretion apparatus in the bacterial membrane
749 and full virulence in vivo. Infect Immun. 2015 Feb 17;IAI.00048-15.

750 20. Koster M, Bitter W, de Cock H, Allaoui A, Cornelis GR, Tommassen J. The outer membrane
751 component, YscC, of the Yop secretion machinery of Yersinia enterocolitica forms a ring-shaped
752 multimeric complex. Mol Microbiol. 1997 Nov;26(4):789–97.

753 21. Daefler S, Russel M. The Salmonella typhimurium InvH protein is an outer membrane
754 lipoprotein required for the proper localization of InvG. Mol Microbiol. 1998 Jun 1;28(6):1367–
755 80.

756 22. Crago A, Koronakis V. Salmonella InvG forms a ring-like multimer that requires the InvH
757 lipoprotein for outer membrane localization. Mol Microbiol. 1998 Oct 1;30(1):47–56.

758 23. Nouwen N, Ranson N, Saibil HR, Wolpensinger B, Engel A, Ghazi A, et al. Secretin PulD:
759 association with pilot PulS, structure, and ion-conducting channel formation. Proc Natl Acad Sci
760 U S A. 1999 Jul 5;96(14):8173–7.

761 24. Schuch R, Maurelli AT. MxiM and MxiJ, base elements of the Mxi-Spa type III secretion system
762 of Shigella, interact with and stabilize the MxiD secretin in the cell envelope. J Bacteriol. 2001
763 Nov 22;183(24):6991–8.

764 25. Burghout P, Beckers F, de Wit E, van Boxtel R, Cornelis GR, Tommassen J, et al. Role of the pilot
765 protein YscW in the biogenesis of the YscC secretin in Yersinia enterocolitica. J Bacteriol. 2004
766 Aug 31;186(16):5366–75.

767 26. Korotkov K V, Gonen T, Hol WGJ. Secretins: dynamic channels for protein transport across
768 membranes. Trends Biochem Sci. 2011 May 9;

769 27. Gu S, Rehman S, Wang X, Shevchik VE, Pickersgill RW. Structural and functional insights into the
770 pilotin-secretin complex of the type II secretion system. PLoS Pathog. 2012;8(2).

771 28. Diepold A, Amstutz M, Abel S, Sorg I, Jenal U, Cornelis GR. Deciphering the assembly of the
772 Yersinia type III secretion injectisome. EMBO J. 2010 Jun 2;29(11):1928–40.

773 29. Diepold A, Wiesand U, Cornelis GR. The assembly of the export apparatus (YscR,S,T,U,V) of the
774 Yersinia type III secretion apparatus occurs independently of other structural components and
775 involves the formation of an YscV oligomer. Mol Microbiol. 2011 Oct 16;82(2):502–14.

776 30. Okon M, Moraes TF, Lario PI, Creagh AL, Haynes CA, Strynadka NC, et al. Structural
777 Characterization of the Type-III Pilot-Secretin Complex from Shigella flexneri. Structure. 2008
778 Oct 8;16(10):1544–54.

779 31. Majewski DD, Okon M, Heinkel F, Robb CS, Vuckovic M, McIntosh LP, et al. Characterization of
780 the Pilotin-Secretin Complex from the Salmonella enterica Type III Secretion System Using
781 Hybrid Structural Methods. Structure. 2021 Feb;29(2):125-138.e5.

782 32. Collin S, Guilvout I, Nickerson NN, Pugsley AP. Sorting of an integral outer membrane protein via
783 the lipoprotein-specific Lol pathway and a dedicated lipoprotein pilotin. Mol Microbiol.
784 2011;80(3):655–65.

785 33. Chami M, Guilvout I, Gregorini M, Rémigy HW, Müller SA, Valerio M, et al. Structural insights
786 into the secretin PulD and its trypsin-resistant core. J Biol Chem. 2005;280(45):37732–41.

787 34. Yin M, Yan Z, Li X. Structural insight into the assembly of the type II secretion system pilotin–
788 secretin complex from enterotoxigenic Escherichia coli. Nat Microbiol. 2018 May 9;3(5):581–7.

789 35. Chernyatina AA, Low HH. Core architecture of a bacterial type II secretion system. Nat Commun.

790 2019;10(1):1–10.

791 36. Hu B, Morado DR, Margolin W, Rohde JR, Arizmendi O, Picking WL, et al. Visualization of the
792 type III secretion sorting platform of Shigella flexneri. Proc Natl Acad Sci. 2015 Jan
793 12;112(4):1047–52.

794 37. Hu B, Lara-Tejero M, Kong Q, Galán JE, Liu J. In Situ Molecular Architecture of the Salmonella
795 Type III Secretion Machine. Cell. 2017 Mar 9;168(6):1065-1074.e10.

796 38. Troisfontaines P, Cornelis GR. Type III Secretion: More Systems Than You Think. Physiology.
797 2005 Oct;20(5):326–39.

798 39. Abby SS, Rocha EPC. The non-flagellar type III secretion system evolved from the bacterial
799 flagellum and diversified into host-cell adapted systems. PLoS Genet. 2012 Sep;8(9):e1002983.

800 40. Iriarte M, Cornelis GR. Identification of SycN, YscX, and YscY, three new elements of the Yersinia
801 yop virulon. J Bacteriol. 1999;181(2):675–80.

802 41. Diepold A, Wiesand U, Amstutz M, Cornelis GR. Assembly of the Yersinia injectisome: the
803 missing pieces. Mol Microbiol. 2012 Sep;85(5):878–92.

804 42. Böhme K, Steinmann R, Kortmann J, Seekircher S, Heroven AK, Berger E, et al. Concerted actions
805 of a thermo-labile regulator and a unique intergenic RNA thermosensor control Yersinia
806 virulence. Isberg RR, editor. PLoS Pathog. 2012 Feb 16;8(2):e1002518.

807 43. Diepold A, Sezgin E, Huseyin M, Mortimer T, Eggeling C, Armitage JP. A dynamic and adaptive
808 network of cytosolic interactions governs protein export by the T3SS injectisome. Nat Commun.
809 2017;8(May):15940.

810 44. Milne-Davies B, Helbig C, Wimmi S, Cheng DWC, Paczia N, Diepold A. Life After Secretion—
811 Yersinia enterocolitica Rapidly Toggles Effector Secretion and Can Resume Cell Division in
812 Response to Changing External Conditions. Front Microbiol. 2019 Sep 13;10:2128.

813 45. Kaniga K, Delor I, Cornelis GR. A wide-host-range suicide vector for improving reverse genetics
814 in Gram-negative bacteria: inactivation of the blaA gene of Yersinia enterocolitica. Gene. 1991
815 Dec 20;109(1):137–41.

816 46. Walker KA, Miller VL. Synchronous Gene Expression of the Yersinia enterocolitica Ysa Type III
817 Secretion System and Its Effectors. J Bacteriol. 2009 Mar 15;191(6):1816–26.

818 47. Mazé A, Glatter T, Bumann D. The central metabolism regulator EIIAGlc switches salmonella
819 from growth arrest to acute virulence through activation of virulence factor secretion. Cell Rep.
820 2014;7(5):1426–33.

821 48. Abrusci P, Vergara-Irigaray M, Johnson S, Beeby MD, Hendrixson DR, Roversi P, et al.
822 Architecture of the major component of the type III secretion system export apparatus. Nat
823 Struct Mol Biol. 2013 Jan 1;20(1):99–104.

824 49. Diepold A, Kudryashev M, Delalez NJ, Berry RM, Armitage JP. Composition, Formation, and
825 Regulation of the Cytosolic C-ring, a Dynamic Component of the Type III Secretion Injectisome.
826 Stock AM, editor. PLOS Biol. 2015 Jan 15;13(1):e1002039.

827 50. Wimmi S, Balinovic A, Jeckel H, Selinger L, Lampaki D, Eisemann E, et al. Dynamic relocalization
828 of cytosolic type III secretion system components prevents premature protein secretion at low
829 external pH. Nat Commun. 2021 Dec 12;12(1):1625.

830 51. Schwiesow L, Lam H, Dersch P, Auerbuch V. Yersinia Type III Secretion System Master Regulator
831 LcrF. Margolin W, editor. J Bacteriol. 2016 Feb 15;198(4):604–14.

832 52. Bange G, Kümmerer N, Engel C, Bozkurt G, Wild K, Sinning I. FlhA provides the adaptor for
833 coordinated delivery of late flagella building blocks to the type III secretion system. Proc Natl

834 Acad Sci U S A. 2010 Jun 21;107(25):11295–300.

835 53. Xing Q, Shi K, Portaliou AG, Rossi P, Economou A, Kalodimos CG. Structures of chaperone-
836 substrate complexes docked onto the export gate in a type III secretion system. Nat Commun.
837 2018 Dec 2;9(1):1773.

838 54. Inoue Y, Kinoshita M, Kida M, Takekawa N, Namba K, Imada K, et al. The FlhA linker mediates
839 flagellar protein export switching during flagellar assembly. Commun Biol. 2021;4(1).

840 55. Sorg I, Wagner S, Amstutz M, Müller SA, Broz P, Lussi Y, et al. YscU recognizes translocators as
841 export substrates of the Yersinia injectisome. EMBO J. 2007 Jun 19;26(12):3015–24.

842 56. Day JB, Plano G V. A complex composed of SycN and YscB functions as a specific chaperone for
843 YopN in Yersinia pestis. Mol Microbiol. 1998 Nov 1;30(4):777–88.

844 57. Botteaux A, Sory M-P, Biskri L, Parsot C, Allaoui A. MxiC is secreted by and controls the
845 substrate specificity of the Shigella flexneri type III secretion apparatus. Mol Microbiol.
846 2009;71(2):449–60.

847 58. Lara-Tejero M, Kato J, Wagner S, Liu X, Galán JE. A Sorting Platform Determines the Order of
848 Protein Secretion in Bacterial Type III Systems. Science (80-). 2011 Feb 2;331(6021):1188–91.

849 59. Schuch R, Maurelli AT. The Mxi-Spa type III secretory pathway of Shigella flexneri requires an
850 outer membrane lipoprotein, MxiM, for invasin translocation. Infect Immun. 1999;67(4):1982–
851 91.

852 60. Jeckelmann JM, Erni B. Transporters of glucose and other carbohydrates in bacteria. Pflugers
853 Arch Eur J Physiol. 2020;472(9):1129–53.

854 61. Pflüger-Grau K, Görke B. Regulatory roles of the bacterial nitrogen-related phosphotransferase
855 system. Trends Microbiol. 2010;18(5):205–14.

856 62. Pacheco AR, Sperandio V. Enteric pathogens exploit the microbiota-generated nutritional
857 environment of the gut. Metab Bact Pathog. 2015;(10):279–96.

858 63. Jeckelmann JM, Erni B. Carbohydrate Transport by Group Translocation: The Bacterial
859 Phosphoenolpyruvate: Sugar Phosphotransferase System. Vol. 92, Subcellular Biochemistry.
860 Springer International Publishing; 2019. 223–274 p.

861 64. Palace SG, Proulx MK, Lu S, Baker RE, Goguen JD. Genome-wide mutant fitness profiling
862 identifies nutritional requirements for optimal growth of Yersinia pestis in deep tissue. MBio.
863 2014;5(4).

864 65. Wang Q, Millet YA, Chao MC, Sasabe J, Davis BM, Waldor MK. A genome-wide screen reveals
865 that the Vibrio cholerae phosphoenolpyruvate phosphotransferase system modulates virulence
866 gene expression. Infect Immun. 2015;83(9):3381–95.

867 66. Kok M, Bron G, Erni B, Mukhija S. Effect of enzyme I of the bacterial phosphoenolpyruvate :
868 Sugar phosphotransferase system (PTS) on virulence in a murine model. Microbiology.
869 2003;149(9):2645–52.

870 67. Collins J, Robinson C, Danhof H, Knetsch CW, Van Leeuwen HC, Lawley TD, et al. Dietary
871 trehalose enhances virulence of epidemic Clostridium difficile. Nature. 2018;553(7688):291–4.

872 68. Carter PB, Zahorchak RJ, Brubaker RR. Plague virulence antigens from Yersinia enterocolitica.
873 Infect Immun. 1980 May;28(2):638–40.

874 69. Sasakawa C, Kamata K, Sakai T, Murayama SY, Makino S, Yoshikawa M. Molecular alteration of
875 the 140-megadalton plasmid associated with loss of virulence and Congo red binding activity in
876 Shigella flexneri. Infect Immun. 1986 Feb;51(2):470–5.

877 70. Sturm A, Heinemann M, Arnoldini M, Benecke A, Ackermann M, Benz M, et al. The cost of
878 virulence: retarded growth of Salmonella Typhimurium cells expressing type III secretion system
879 1. PLoS Pathog. 2011 Jul;7(7):e1002143.

880 71. Gur E, Sauer RT. Recognition of misfolded proteins by Lon, a AAA+ protease. Genes Dev.
881 2008;22(16):2267–77.

882 72. Tsilibaris V, Maenhaut-Michel G, Van Melderen L. Biological roles of the Lon ATP-dependent
883 protease. Res Microbiol. 2006;157(8):701–13.

884 73. Omnus DJ, Fink MJ, Szwedo K, Jonas K. The lon protease temporally restricts polar cell
885 differentiation events during the caulobacter cell cycle. Elife. 2021;10:1–24.

886 74. Cornelis GR, Sluiters C, Delor I, Geib D, Kaniga K, de Rouvroit CL, et al. ymoA, a Yersinia
887 enterocolitica chromosomal gene modulating the expression of virulence functions. Mol
888 Microbiol. 1991 May;5(5):1023–34.

889 75. Cornelis GR. Role of the Transcription Activator VirF and the Histone-like Protein YmoA in the
890 Thermoregulation of Virulence Functions in Yersiniae. Zentralblatt fur Bakteriol. 1993;278(2–
891 3):149–64.

892 76. Jackson MW, Silva-Herzog E, Plano G V. The ATP-dependent ClpXP and Lon proteases regulate
893 expression of the Yersinia pestis type III secretion system via regulated proteolysis of YmoA, a
894 small histone-like protein. Mol Microbiol. 2004;54(5):1364–78.

895 77. Breidenstein EBM, Janot L, Strehmel J, Fernandez L, Taylor PK, Kukavica-Ibrulj I, et al. The Lon
896 Protease Is Essential for Full Virulence in Pseudomonas aeruginosa. PLoS One. 2012;7(11).

897 78. Bretz J, Losada L, Lisboa K, Hutcheson SW. Lon protease functions as a negative regulator of
898 type III protein secretion in Pseudomonas syringae. Mol Microbiol. 2002;45(2):397–409.

899 79. Zhou X, Teper D, Andrade MO, Zhang T, Chen S, Song WY, et al. A phosphorylation switch on lon
900 protease regulates bacterial type iii secretion system in host. MBio. 2018;9(1).

901 80. Lee JH, Ancona V, Zhao Y. Lon protease modulates virulence traits in Erwinia amylovora by
902 direct monitoring of major regulators and indirectly through the Rcs and Gac-Csr regulatory
903 systems. Mol Plant Pathol. 2018;19(4):827–40.

904 81. Figaj D, Czaplewska P, Przepióra T, Ambroziak P, Potrykus M, Skorko-Glonek J. Lon protease is
905 important for growth under stressful conditions and pathogenicity of the phytopathogen,
906 bacterium Dickeya solani. Int J Mol Sci. 2020;21(10).

907 82. Renault TT, Guse A, Erhardt M. Export Mechanisms and Energy Transduction in Type-III
908 Secretion Machines. In: Current Topics in Microbiology and Immunology. Springer, Berlin,
909 Heidelberg; 2019. p. 1–17.

910 83. Konovalova A, Silhavy TJ. Outer membrane lipoprotein biogenesis: Lol is not the end. Philos
911 Trans R Soc B Biol Sci. 2015;370(1679).

912 84. Kudryashev M, Stenta M, Schmelz S, Amstutz M, Wiesand U, Castaño-Díez D, et al. In situ
913 structural analysis of the Yersinia enterocolitica injectisome. Elife. 2013 Jan;2(Im):e00792.

914 85. Lambert de Rouvroit C, Sluiters C, Cornelis GR. Role of the transcriptional activator, VirF, and
915 temperature in the expression of the pYV plasmid genes of Yersinia enterocolitica. Mol
916 Microbiol. 1992 Feb;6(3):395–409.

917 86. Schindelin J, Arganda-Carreras I, Frise E, Kaynig V, Longair M, Pietzsch T, et al. Fiji: an open-
918 source platform for biological-image analysis. Nat Methods. 2012 Jul 28;9(7):676–82.

919 87. Thevenaz P, Ruttimann UE, Unser M. A pyramid approach to subpixel registration based on
920 intensity. IEEE Trans Image Process. 1998;7(1):27–41.

921 88. Spahn C, Laine RF, Pereira P, Gómez-de-mariscal E. Supplementary information - DeepBacs :
922 Bacterial image analysis using open-source deep learning approaches. bioRxiv. 2021;1–15.

923 89. Cox J, Mann M. MaxQuant enables high peptide identification rates, individualized p.p.b.-range
924 mass accuracies and proteome-wide protein quantification. Nat Biotechnol. 2008 Dec
925 30;26(12):1367–72.

926 90. Fuchs TM, Brandt K, Starke M, Rattei T. Shotgun sequencing of Yersinia enterocolitica strain
927 W22703 (biotype 2, serotype O:9): Genomic evidence for oscillation between invertebrates and
928 mammals. BMC Genomics. 2011;12:1–14.

929 91. Glatter T, Ludwig C, Ahrné E, Aebersold R, Heck AJR, Schmidt A. Large-scale quantitative
930 assessment of different in-solution protein digestion protocols reveals superior cleavage
931 efficiency of tandem Lys-C/trypsin proteolysis over trypsin digestion. J Proteome Res.
932 2012;11(11).

933 92. Ahrné E, Glatter T, Viganò C, Von Schubert C, Nigg EA, Schmidt A. Evaluation and improvement
934 of quantification accuracy in isobaric mass tag-based protein quantification experiments. J
935 Proteome Res. 2016;15(8):2537–47.

936 93. Tyanova S, Temu T, Sinitcyn P, Carlson A, Hein MY, Geiger T, et al. The Perseus computational
937 platform for comprehensive analysis of (prote)omics data. Nat Methods. 2016;13(9):731–40.

938 94. Lampaki D, Diepold A, Glatter T. A Serial Sample Processing Strategy with Improved
939 Performance for in-Depth Quantitative Analysis of Type III Secretion Events in Pseudomonas
940 aeruginosa. J Proteome Res. 2020 Jan 3;19(1):543–53.

941 95. Wallace IM, O'Sullivan O, Higgins DG, Notredame C. M-Coffee: combining multiple sequence
942 alignment methods with T-Coffee. Nucleic Acids Res. 2006;34:1692–9.

943 96. Erhardt M, Namba K, Hughes KT. Bacterial nanomachines: the flagellum and type III injectisome.
944 Cold Spring Harb Perspect Biol. 2010 Nov 1;2(11):a000299.

945 97. Hueck CJ. Type III protein secretion systems in bacterial pathogens of animals and plants.
946 Microbiol Mol Biol Rev. 1998 Jun;62(2):379–433.

947 98. Wagner S, Diepold A. A Unified Nomenclature for Injectisome-Type Type III Secretion Systems.
948 In: Current topics in microbiology and immunology. 2020. p. 427: 1-10.

949